Available online at www.sciencedirect.com
ScienceDirect
Journal of Sound and Vibration 321 (2009) 137–165
JOURNAL OF SOUND AND VIBRATION
www.elsevier.com/locate/jsvi

Wave beaming and wave propagation in light weight plates with truss-like cores

Torsten Kohrs*, Björn A.T. Petersson

Institute of Fluid Mechanics and Engineering Acoustics, Technische Universität Berlin, Einsteinufer 25, 10587 Berlin, Germany

Received 3 May 2008; received in revised form 24 August 2008; accepted 9 September 2008
Handling Editor: C.L. Morfey
Available online 13 November 2008

Abstract

Wave propagation in light weight plates with truss-like cores is investigated. For generic light weight plates with periodicity in one dimension the wavenumber content is characterized by strong directional wave propagation. Also wave beaming results in some frequency bands, where local vibrations are of primary concern. The strong periodic pass- and stop-band behaviour detected previously for profile strips is transformed into a spatial stop- and pass-band distribution of high and low vibration zones. As a result, the stop-bands of the two-dimensional investigation are weakened for point excitation of full plates. This is manifested by a rising real part of the input mobilities. In these lateral stop-bands the imparted power is transmitted mainly in the direction parallel to the webs of the inner core. In the low frequency region, where global plate waves dominate, the vibrational behaviour can be reduced to equivalent plate models. For profiles with inclined webs, global orthotropicity is limited and global bending wave dispersion is similar irrespective of direction. For profiles with solely vertical webs, strong orthotropicity with significantly higher wavenumbers in the lateral direction, normal to the webs, is demonstrated.

Different methods for the extraction of theoretical and experimental dispersion characteristics of the plates are applied and discussed. The theoretical dispersion characteristics are validated on a regional train floor section which serves as an application example.

1. Introduction

Wave propagation in light weight profile strips with different truss-like core geometries is thoroughly investigated in Ref. [1]. Typical periodic system effects like pass- and stop-band behaviour are identified. The results presented there are valid also for plates with line force excitation perpendicular to the strip plane in the direction parallel to the intermediate core plates. In this paper the wave propagation in the light weight plates illustrated in Fig. 1 is investigated. Studies on the two-dimensional mid- and high frequency wave propagation in such light weight plates are rare and have not dealt with the occurrence of periodic system effects.

For structure-borne sound applications the loads are often concentrated to small areas where, e.g. machine footings are attached to the light weight plate. As long as the wavelength is larger than the contact dimension

*Corresponding author.
E-mail address: torsten.kohrs@tu-berlin.de (T. Kohrs).

0022-460X/$ - see front matter © 2008 Elsevier Ltd. All rights reserved.
doi:10.1016/j.jsv.2008.09.033

Nomenclature

f	frequency
j	$\sqrt{-1}$
k	wavenumber
l_x	length of subelement
n, p, q	integer values
t	thickness
v	velocity
A, B, C	labels for investigated generic profiles
E_0	Young's modulus
L	length of finite strips A–C
L_e	periodic length
N	number of sampling points
V	velocity spectrum (wavenumber domain)
$\mathbf{0}$	zero matrix or vector
$\mathbf{A}, \mathbf{B}$	reduction matrices
$\mathbf{F}$	force vector
$\mathbf{I}$	identity matrix
$\mathbf{K}$	dynamic stiffness matrix
$\mathbf{M}$	mass matrix
$\mathbf{S}$	stiffness matrix
$\mathbf{T}$	transfer matrix
α	web angle
ε	phase constant
η	loss factor
λ	eigenvalue
μ	propagation constant
ν	Poisson's ratio
ρ	mass density
ω	circular frequency
$\boldsymbol{\xi}$	displacement vector
$\boldsymbol{\phi}$	right eigenvector
$\boldsymbol{\Phi}$	right eigenvector matrix

Indexes

b	back
e	element
f	front
i	index
l	left
r	right
x	x-direction
y	y-direction
z	z-direction

Superscripts

-1	matrix inverse
T	matrix transpose
H	matrix Hermitian transpose (complex conjugate and transpose)

they can be treated as point contacts. For the case of point force excitation the wave propagation spreading from the excitation point is treated in Sections 2 and 3. One of the questions posed is if the pass- and stop-band effects are also distinct for point excited plate configurations. Langley and Bardell show in Ref. [2] that for two-dimensional periodic systems (beam grillages), the wave propagation can be highly directional. Similar results are reported by Ruzzene et al. [3]. It is investigated here whether such a phenomenon also exists for a two-dimensional structure with periodicity only in one direction. Therefore the forced response of typical profiles is calculated using standard finite element techniques. For a physical understanding and interpretation of the wave propagation in the light weight profiles, the two-dimensional wavenumber content is extracted from the calculated vibration fields. Results of the spatial Fourier-transform method are shown and reveal the wave beaming effects for the investigated light weight plates. As an alternative to the spatial Fourier transform the dispersion characteristics of propagating waves can be extracted from a single subelement, repeated in both directions, resulting in the so-called phase constant surfaces. Results are compared with DFT and reveal the enhanced resolution capabilities of the subelement approach for periodic profiles. For profiles of finite width the wavenumber content is extracted using the waveguide finite element (WFE) technique, [4,5]. A narrow slice of the complete waveguide is modelled with standard FE methods and periodic system theory delivers the characteristic waves propagating in the z-direction in the infinite light weight plate section.

2. Dispersion characteristics using DFT

In order to understand the wave propagation in the light weight profiles, the wavenumber content for propagation in the x- and z-direction is sought (see Fig. 1). There are several options to extract the

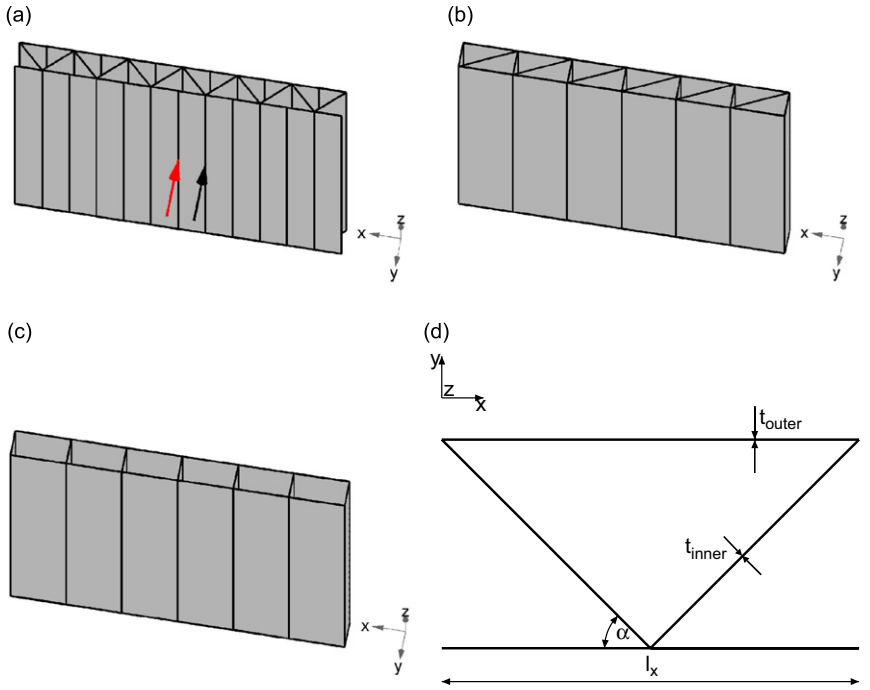

Fig. 1. Cut-outs of investigated generic light weight profiles and nomenclature: (a) profile A, (b) profile B, (c) profile C (d) nomenclature for subelement dimensions. Arrows in (a) indicate the extreme normal force excitation positions (left arrow at centre of plate strip and right arrow at a stiffener position). Coordinate nomenclature: x: width; y: height; z: length.

wavenumber content from measured or calculated data. A lot of work in the area of one-dimensional wavenumber estimation has been published, see, e.g. Refs. [6–8]. For two-dimensional extraction procedures details can be found in Refs. [9–11]. Mainly for usage with experimental data a correlation method [10] and the inhomogeneous wave correlation (IWC) method [9,12] are introduced. Both are intended to overcome some limitations of the standard spatial discrete Fourier transform technique when only limited and possibly noisy (experimental) data is available. For this study calculated vibration fields with high resolution are available so that the spatial discrete Fourier transform (DFT) technique is applicable. A clearer picture of the two-dimensional wave propagation can be gained with the evaluation of the phase constant surfaces from the two-dimensional-periodic subelement. This is compared with the DFT results in Section 3. If the system can be handled as a waveguide, in which wave propagation is of primary concern only along the waveguide, i.e. parallel to the inner webs of the profile, the dispersion characteristics for this direction can be investigated, e.g. with spectral or WFE techniques, see, e.g. Refs. [4,5,13]. From these methods the properties of characteristic waves propagating in the waveguide direction can be deduced. For profiles of finite width this approach is favourable for investigations of wave propagation in the waveguide direction. This approach is chosen for the investigation in Section 4. The IWC method is applied for the experimental dispersion investigation of a train floor in Section 5.2 and results are related to the DFT results.

2.1. Discrete spatial Fourier transform

For the application of the DFT-method, a spatial sampling at points on a discrete two-dimensional grid is necessary, resulting in the two-dimensional discrete Fourier transform. Having a profile section of dimensions L_x and L_z with $N_x \times N_z$ equally distributed spatial sampling points $v_{n_x,n_z} = v(n_x\Delta x, n_z\Delta z), n_x = 1,2,3,\ldots,N_x; n_z = 1,2,3,\ldots,N_z$, results in the following transformation:

$$V_{p,q} = V(p\Delta k_x, q\Delta k_z) = \Delta x\Delta z \sum_{n_x=1}^{N_x}\sum_{n_z=1}^{N_z} v_{n_x,n_z}\, \mathrm{e}^{-\mathrm{j}\, p\Delta k_x\, x_p}\, \mathrm{e}^{-\mathrm{j}\, q\Delta k_z\, z_q},$$

Table 1
Geometry and material properties of investigated profiles

Profile	A	B	C
t_{outer} (mm)	3.0	3.0	3.0
t_{inner} (mm)	3.0	2.6	8.5
Web angle α (deg)	45.0	26.6/90.0	90.0
Periodic length l_x (mm)	100	100	100
Total length L_x (mm)	3000	3000	3000
Total length L_z (mm)	5000	5000	5000
E_0 (N/m^2)	7.2×10^{10}	7.2×10^{10}	7.2×10^{10}
ν (–)	0.34	0.34	0.34
η (–)	0.01/0.1	0.01/0.1	0.01/0.1
ρ (kg/m^3)	2700	2700	2700
Total mass per unit area (kg/m^2)	27.7	27.7	27.7

$$\Delta k_x = \frac{2\pi}{L_x}, \quad \Delta k_z = \frac{2\pi}{L_z}. \tag{1}$$

This is a direct extension of the one-dimensional spatial Fourier transform applied in Ref. [1], where limitations and practical aspects of the method and its application are discussed. As stated already for the one-dimensional case, the DFT-approach is beneficial for a specific forced excitation, as it directly results in the energy distribution among different waves for this excitation. On the other hand this can be a limitation if a more general understanding of possible wave propagation in the light weight plates is sought. It cannot be directly assured that all the important wave types are excited and hence can be extracted. For a more general investigation, the WFE method or the phase constant surface evaluation presented later on proves more appropriate.

The velocity field data on a regular spaced grid is calculated using standard FE-modelling techniques using MSC NASTRAN.[1] In order to suppress reflections from the model boundaries, the edge regions (0.5 m width) are highly damped (loss factor 0.1). For a reduced calculation effort, symmetry is exploited and only a quarter model with symmetry boundary conditions is established. The principal geometries of the investigated profile cores are shown in Fig. 1. Details of geometric dimensions and material properties are listed in Table 1. The thickness of the inner webs of profiles B and C is adjusted to maintain constant total mass per unit area.

As shown already in Ref. [1] the vibrations of truss-like light weight objects can be divided in global and local wave motion. The global waves dominate at lower frequencies whereas at higher frequencies both global and local vibrations are of significance.

The geometry of the truss-like light weight profiles is highly orthotropic as the intermediate plates are orientated only in the z-direction. Despite this geometrical orthotropicity, the global vibrations for profiles of type A are mainly isotropic as shown in Ref. [14]. The static and low frequency bending stiffnesses are dominated by the face plates which do not comprise any orthotropicity. The investigation sheds some light on the influence of generic geometry (A, B, C) on vibrational orthotropicity.

Representative for the global wave region, the 400 Hz results for all three profile types are presented in Fig. 2. The wavenumber content is displayed on a logarithmic grey scale and strong contributions are dark shaded. The results presented correspond to unit normal point force excitation at the centre of a plate field (A and C) or an excitation at a stiffener position (B). The normal velocity of the outer plate of the excited side is selected for the evaluation. The influence of excitation position is treated in Ref. [15] and Section 2.2 and can be summarized by a quantitative variation in the wavenumber content, but the inherent waves are similar.

The results in Fig. 2 show the dominance of the global, low wavenumber waves for all profiles at 400 Hz. The response of A and B is similar, the wavenumber content displaying the isotropic nature of the wave propagation with a quarter circle at very low wavenumbers. In contrast to this the velocity field for profile C

[1]CQUAD4 shell elements, element length 12.5 mm, frequency limit according to six elements per (bending) wavelength criterion is about 5300 Hz, direct frequency response calculation method (SOL 108) is used.

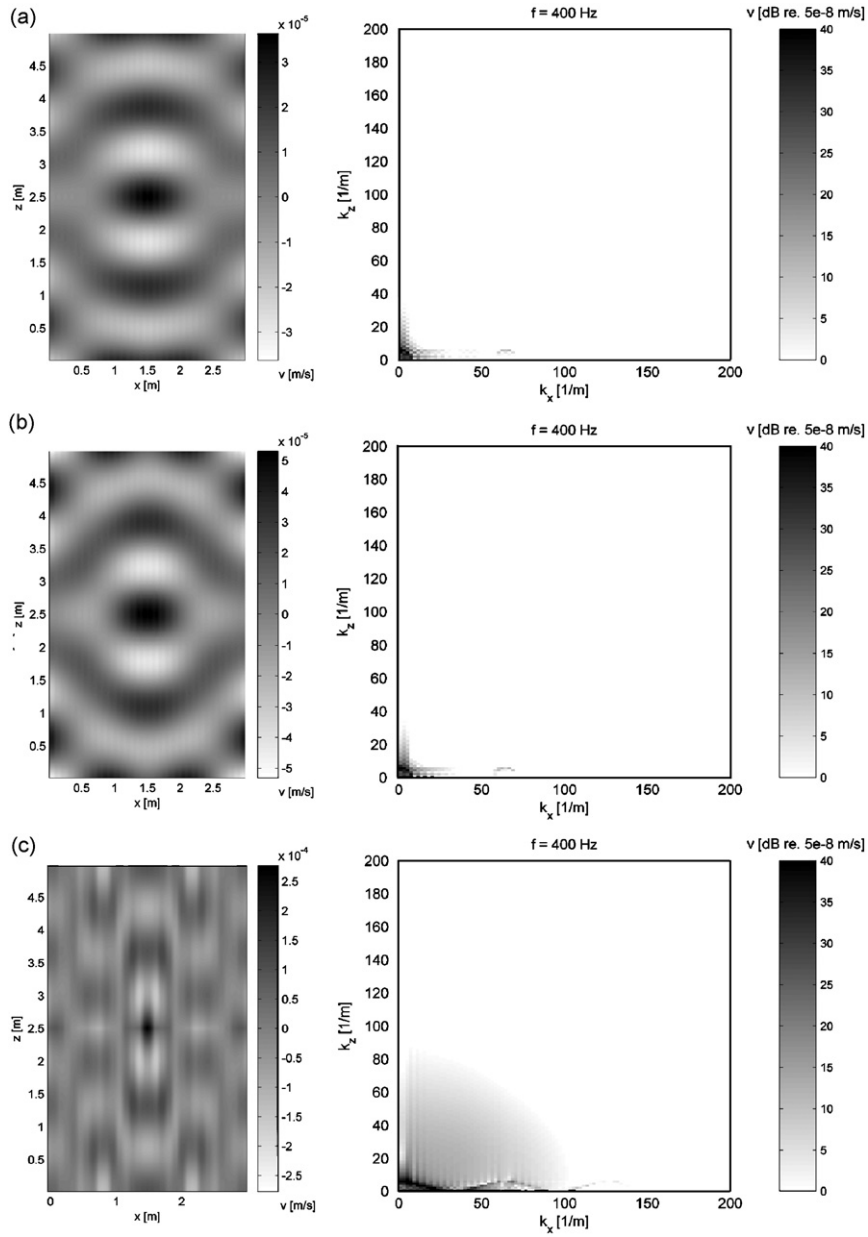

Fig. 2. Velocity fields for normal force excitation (left) and DFT wavenumber content (right) ($f = 400\,\mathrm{Hz}$). (a) Profile A, plate field excitation, (b) profile B, stiffener excitation and (c) profile C, plate field excitation.

comprises much shorter wavelength in the x-direction ($k_x = 30\,\mathrm{m}^{-1}$, $k_z = 8\,\mathrm{m}^{-1}$, see Fig. 2(c)). This is directly reflected by the elliptical wavenumber curve in the DFT result with a higher wavenumber for k_x.

Although the global waves dominate the vibration, there are also higher wavenumber components included, representing some local behaviour. For the periodicity in the x-direction, a higher wavenumber component is present with a distance of $2\pi/l_x = 62.8\,\mathrm{m}^{-1}$ to the global waves, where l_x is the periodic length of 0.1 m in the x-direction.

At high frequencies the significance of the global waves decreases (Fig. 3) and the velocity field is dominated by high wavenumber (short wavelength) components. These wavenumber components comprise an interesting feature. They propagate only in the direction of a limited angular segment, which is related to strong wave

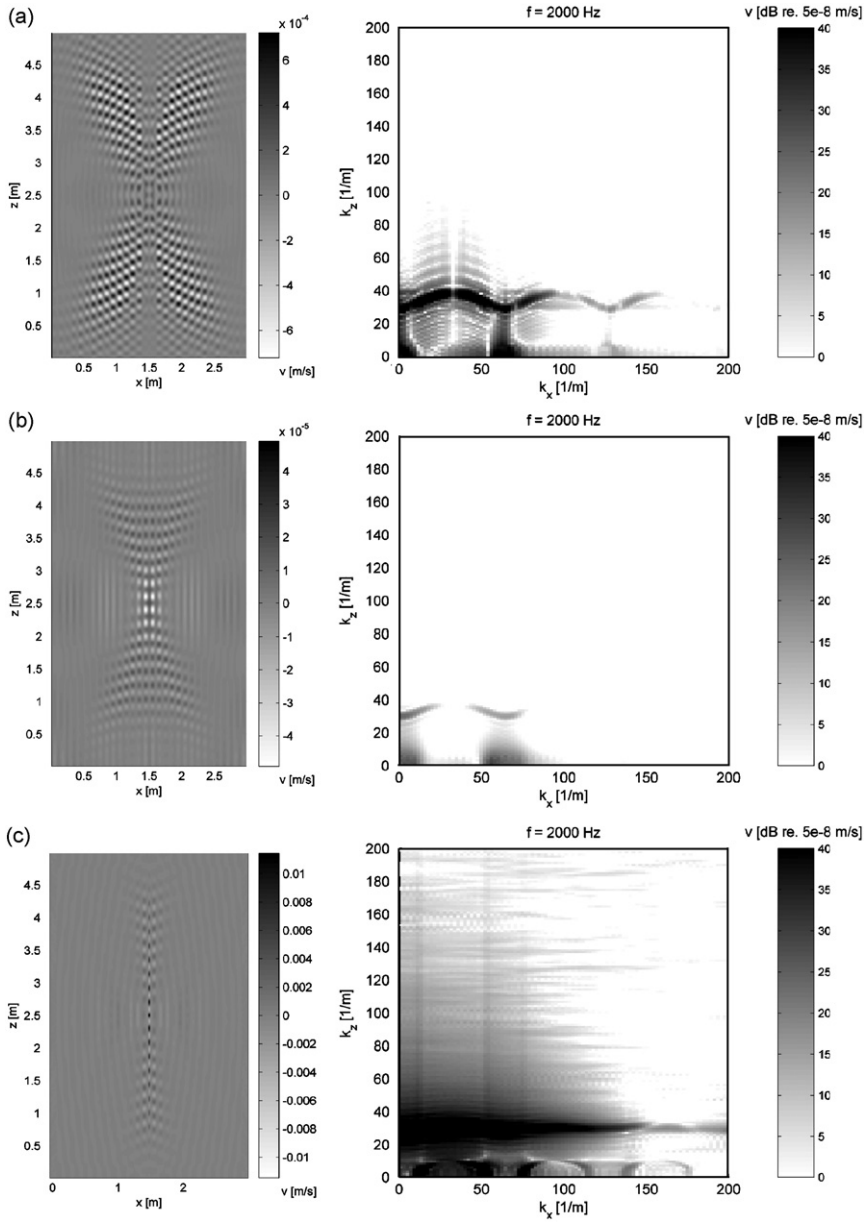

Fig. 3. Velocity fields for normal force excitation (left) and DFT wavenumber content (right) ($f = 2000$ Hz). (a) Profile A, plate field excitation, (b) profile B, stiffener excitation and (c) profile C, plate field excitation.

beaming effects most clearly visible for types A and C. For profile A the main direction is oblique, whereas for profile C the lobes are orientated mainly in the z-direction. This kind of wave beaming is similar to the results presented by Langley [2,16] for point excited periodic beam grillages. This means that wave beaming is not only existing for structures with periodicity in both directions, but also for structures comprising periodicity only in one direction.

At still higher frequencies the wave propagation characteristics shown in Fig. 4 for 5000 Hz arise. For profile A strong wave beaming effects are still visible. The wave propagation in profile C arises mainly along the excited plate strip in the z-direction. Nonetheless, some less pronounced waves with periodic wavenumber content propagate also in the x-direction, clearly visible in the wavenumber domain.

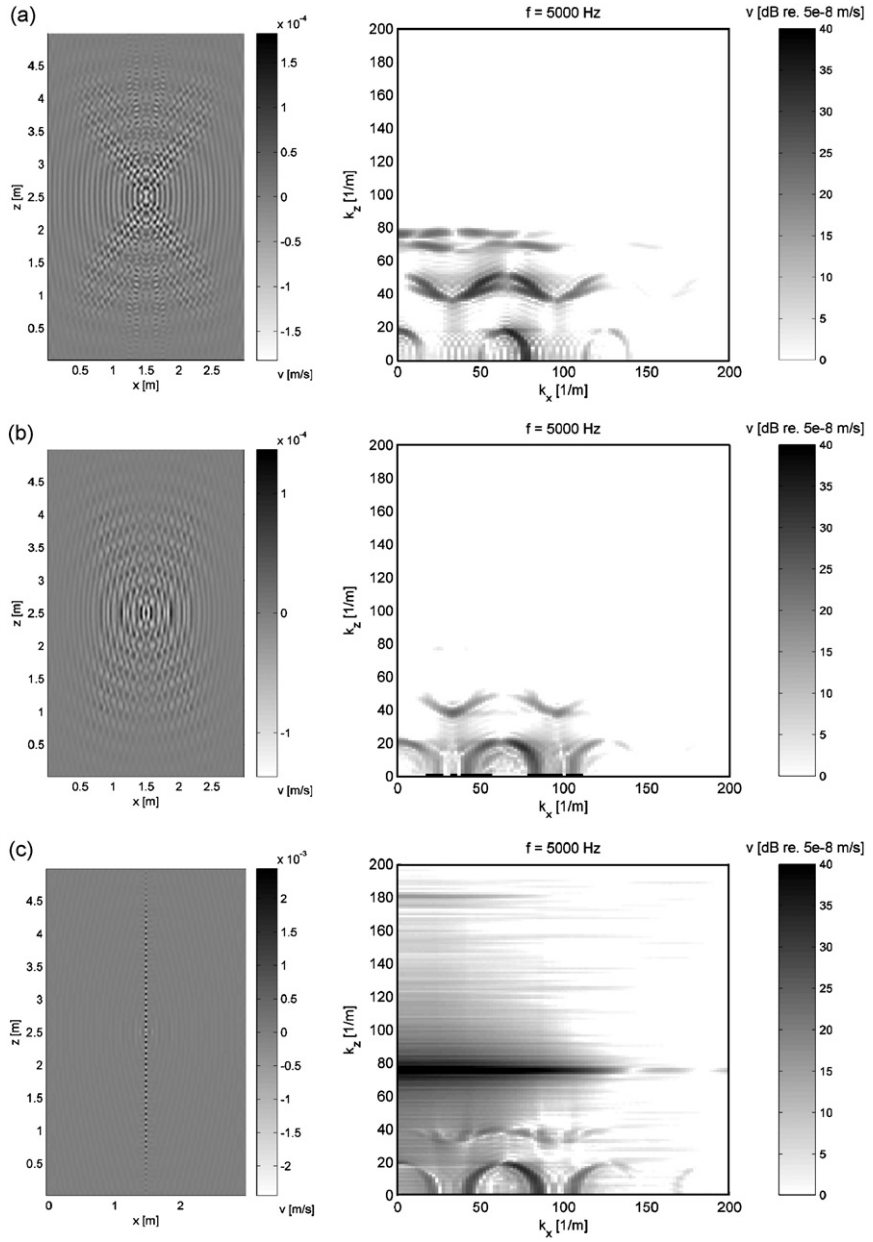

Fig. 4. Velocity fields for normal force excitation (left) and DFT wavenumber content (right) ($f = 5000$ Hz). (a) Profile A, plate field excitation, (b) profile B, stiffener excitation and (c) profile C, plate field excitation.

2.2. Frequency dependent dispersion from DFT

In order to get insight into the frequency dependent behaviour and for comparison with WFE and phase constant surface results, the wavenumbers in the main directions x and z are extracted from the two-dimensional-DFT results. The extraction procedure is performed with a frequency increment of 50 Hz and results are shown with a shaded grey scale in Figs. 5–7 for the different generic profiles and excitation positions. For comparison, the plots include the results of the phase constant surface investigation presented in Section 3 with full black lines. As expected the dispersion in the x-direction is very similar to

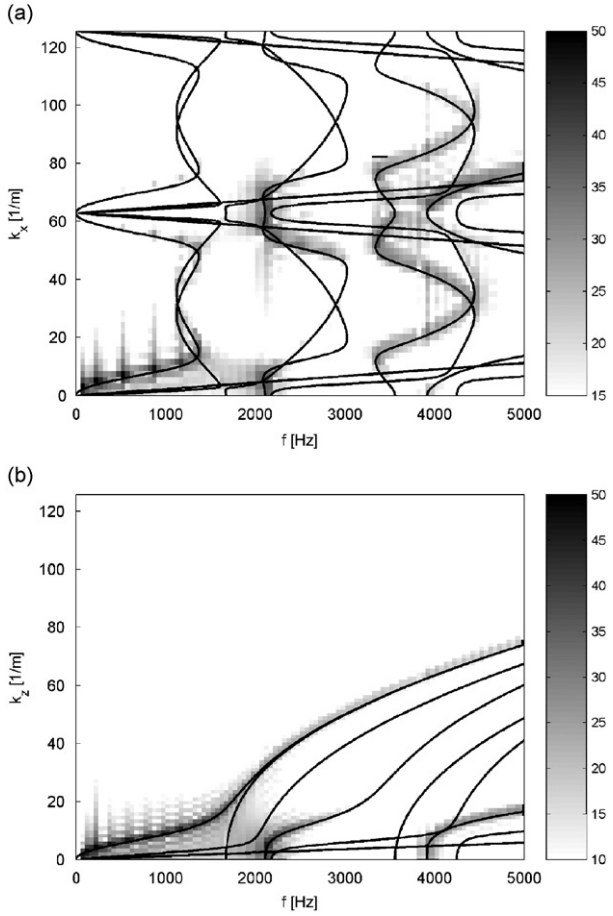

Fig. 5. Dispersion characteristics of profile A extracted from the phase constant surfaces in (a) the x- and (b) the z-direction and DFT results with shaded grey scale [dB re. $5e-8\,\mathrm{m/s}$]. DFT results for normal unit force excitation at stiffener position.

the characteristics obtained from the two-dimensional strip investigation presented in Ref. [1]. The periodic stop- and pass-band behaviour is distinct especially for profile C with two wide stop-bands (400–1600 Hz and 2200–4100 Hz). Moreover the periodic wavenumber content with spacing $2\pi/l_x$ is clearly visible in the pass-bands.

The influence of force position is studied and the results, not included for the sake of brevity, reveal that the same waves are inherent in the structure independent of excitation position but with different amplitudes. The plate field excitation tends to excite higher wavenumbers, i.e. local waves, than the stiffener excitation.

As expected by the plate geometries, wave propagation in the x-direction is highly influenced by the structural periodicity and, to different extents, stop- and pass-band behaviour is observed. Wave propagation in the z-direction, parallel to the intermediate plates, is much more distinct and exists in the complete frequency range. It starts with global bending wave behaviour at low frequencies and experiences a transition to local plate strip bending wave behaviour at high frequencies. This is similar to, e.g. dispersion in cylinders, where global torsional and bending waves of the complete cylinder dominate at low frequencies and change to bending dispersion of the hull at high frequencies.

The limited resolution of the DFT results makes the interpretation somewhat difficult. The WFE method and the phase constant surface results will give some further insight into the wave propagation in the z-direction and the corresponding characteristic waves.

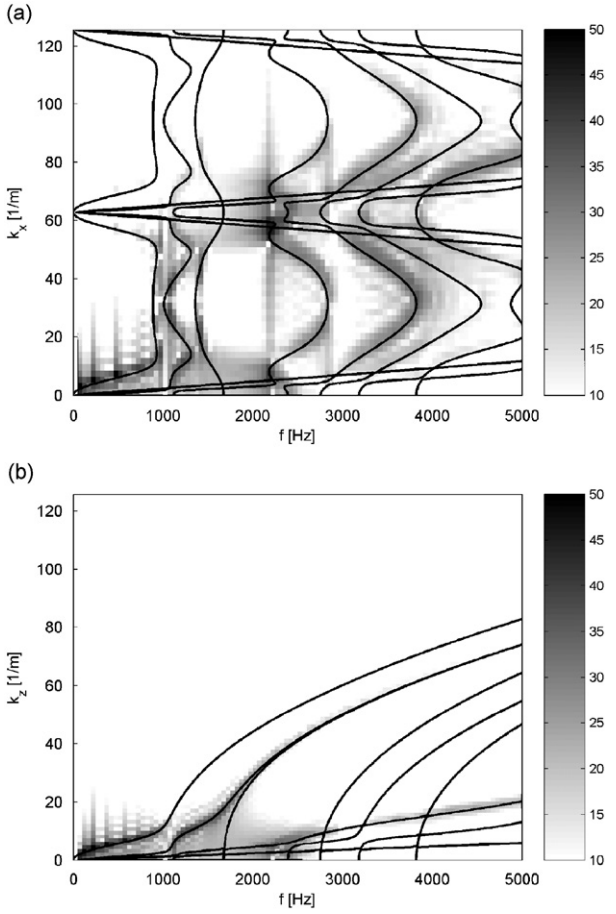

Fig. 6. Dispersion characteristics of profile B extracted from the phase constant surfaces in (a) the x- and (b) the z-direction and DFT results with shaded grey scale [dB re. $5e-8$ m/s]. DFT results for normal unit force excitation at stiffener position.

3. Dispersion characteristics using phase constant surfaces

3.1. Theory

Based on two-dimensional-periodic system theory the so-called phase constant surfaces can be extracted from a reduced eigenvalue problem of the two-dimensional-periodic subelement [2,17,18].

The naming convention for the subelement used for extraction of the phase constant surfaces is shown in Fig. 8. In contrast to the formulation by Mead et al. [17], no inner degrees of freedom (dof) and no dof solely related to the left and right boundaries are present. This is due to the fact that the extension in the z-direction is intended to be very small in order to achieve a high limiting wavenumber in this non-periodic direction.

Starting with the definition of the displacement and force vectors,

$$\boldsymbol{\xi} = [\boldsymbol{\xi}_b \boldsymbol{\xi}_f \boldsymbol{\xi}_{lf} \boldsymbol{\xi}_{lb} \boldsymbol{\xi}_{rb} \boldsymbol{\xi}_{rf}]^{\mathrm{T}}, \tag{2}$$

$$\mathbf{F} = [\mathbf{F}_b \mathbf{F}_f \mathbf{F}_{lf} \mathbf{F}_{lb} \mathbf{F}_{rb} \mathbf{F}_{rf}]^{\mathrm{T}}, \tag{3}$$

the undamped equations of motion with stiffness matrix $\mathbf{S}$ and mass matrix $\mathbf{M}$ read:

$$(\mathbf{S} - \omega^2 \mathbf{M})\boldsymbol{\xi} = \mathbf{F}. \tag{4}$$

Using Bloch's theorem relating displacement and forces at the boundaries of the periodic subelement, the equations of motion can be condensed in the case of free wave propagation. The detailed Bloch conditions

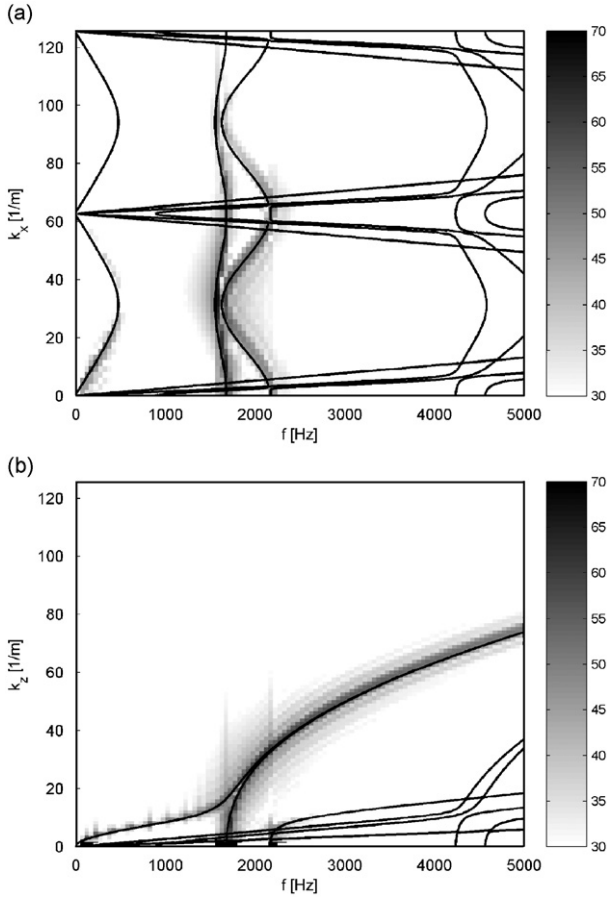

Fig. 7. Dispersion characteristics of profile C extracted from the phase constant surfaces in (a) the x- and (b) the z-direction and DFT results with shaded grey scale [dB re. $5e-8\,\mathrm{m/s}$]. DFT results for normal unit force excitation at centre of plate field.

read

$$\begin{aligned}
\boldsymbol{\xi}_b &= \mathrm{e}^{\mu_z}\boldsymbol{\xi}_f,\\
\boldsymbol{\xi}_{lb} &= \mathrm{e}^{\mu_z}\boldsymbol{\xi}_{lf},\\
\boldsymbol{\xi}_{rb} &= \mathrm{e}^{\mu_x+\mu_z}\boldsymbol{\xi}_{lf},\\
\boldsymbol{\xi}_{rf} &= \mathrm{e}^{\mu_x}\boldsymbol{\xi}_{lf},
\end{aligned} \tag{5}$$

$$\begin{aligned}
\mathbf{F}_b &= -\mathrm{e}^{\mu_z}\mathbf{F}_f,\\
\mathbf{F}_{lb} &= -\mathrm{e}^{\mu_z}\mathbf{F}_{lf},\\
\mathbf{F}_{rb} &= +\mathrm{e}^{\mu_x+\mu_z}\mathbf{F}_{lf},\\
\mathbf{F}_{rf} &= -\mathrm{e}^{\mu_x}\mathbf{F}_{lf}.
\end{aligned} \tag{6}$$

Using these conditions, reduced vectors can be used

$$\boldsymbol{\xi}_{\mathrm{red}} = [\boldsymbol{\xi}_f\,\boldsymbol{\xi}_{lf}]^{\mathrm{T}}, \tag{7}$$

$$\mathbf{F}_{\mathrm{red}} = [\mathbf{F}_f\,\mathbf{F}_{lf}]^{\mathrm{T}}. \tag{8}$$

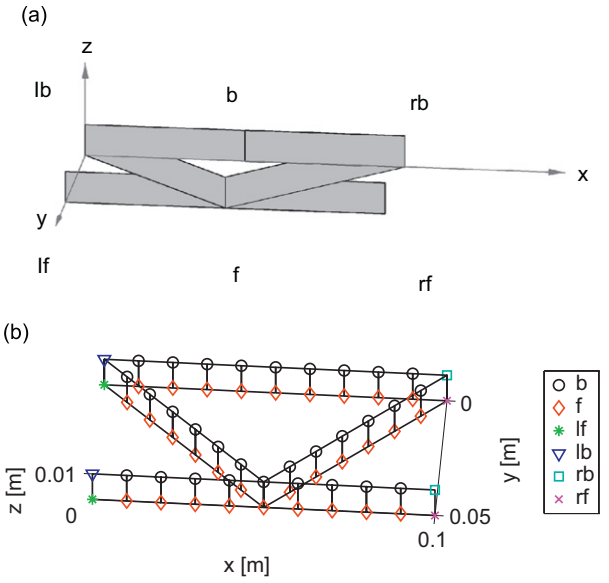

Fig. 8. Naming conventions of the periodic subelement for the dispersion extraction in the x- and the z-direction exemplified for profile A: (a) general illustration and (b) detailed assignment of FE-nodes.

From the reduced vectors the full vectors can be calculated using the Bloch conditions in matrix form,

$$\boldsymbol{\xi} = \mathbf{A}\boldsymbol{\xi}_{\mathrm{red}} \quad \text{with } \mathbf{A} = \begin{pmatrix} \mathbf{I}_b\, \mathrm{e}^{\mu_z} & \mathbf{0} \\ \mathbf{I}_f & \mathbf{0} \\ \mathbf{0} & \mathbf{I}_{lf} \\ \mathbf{0} & \mathbf{I}_{lb}\, \mathrm{e}^{\mu_z} \\ \mathbf{0} & \mathbf{I}_{rb}\, \mathrm{e}^{\mu_x+\mu_z} \\ \mathbf{0} & \mathbf{I}_{rf}\, \mathrm{e}^{\mu_x} \end{pmatrix}, \tag{9}$$

$$\mathbf{F} = \mathbf{B}\mathbf{F}_{\mathrm{red}} \quad \text{with } \mathbf{B} = \begin{pmatrix} -\mathbf{I}_b\, \mathrm{e}^{\mu_z} & \mathbf{0} \\ \mathbf{I}_f & \mathbf{0} \\ \mathbf{0} & \mathbf{I}_{lf} \\ \mathbf{0} & -\mathbf{I}_{lb}\, \mathrm{e}^{\mu_z} \\ \mathbf{0} & +\mathbf{I}_{rb}\, \mathrm{e}^{\mu_x+\mu_z} \\ \mathbf{0} & -\mathbf{I}_{rf}\, \mathrm{e}^{\mu_x} \end{pmatrix}. \tag{10}$$

Introducing the reduced force and velocity vectors in Eq. (4) and pre-multiplying with $\mathbf{A}^{\mathrm{H}}$ results in a reduced eigenvalue problem with reduced mass and stiffness matrices $\mathbf{M}_{\mathrm{red}}$ and $\mathbf{S}_{\mathrm{red}}$.

$$(\mathbf{S}_{\mathrm{red}} - \omega^2\mathbf{M}_{\mathrm{red}})\boldsymbol{\xi}_{\mathrm{red}} = \mathbf{0}, \tag{11}$$

with

$$\mathbf{S}_{\mathrm{red}} = \mathbf{A}^{\mathrm{H}}\mathbf{S}\mathbf{A}, \quad \mathbf{M}_{\mathrm{red}} = \mathbf{A}^{\mathrm{H}}\mathbf{M}\mathbf{A}.$$

The right side of Eq. (11) is $\mathbf{0}$ for purely imaginary propagation constants, i.e. purely propagating waves without losses. For each combination of purely imaginary μ_x, μ_z several real eigenvalue solutions for ω^2 exist. The resulting triples μ_x, μ_z, ω form the so called phase constant surfaces representing the dispersion characteristics of the infinite profile formed by repeated subelements in the x- and z-direction.

3.2. Numerical results

Phase constant surfaces are calculated from FE-subelement models of profiles A, B and C with a mesh size of 10 mm (see Fig. 9).

As the phase constant surfaces are difficult to interpret directly, contours for selected frequencies are presented in Fig. 10. The contour lines represent the wavenumber content for these selected frequencies. Periodicity in the x-direction is accounted for in the plotted results by including higher space harmonics up to $k_x = 200\,\mathrm{m}^{-1}$. For comparison, the DFT results of Section 2.1 are included by colour shading in the plots, while the contour lines are included with dark full lines. The agreement between DFT results and contour lines is high. The comparison of the phase constant surface dispersion results with the spatial Fourier transform results reveals the strength of the former to identify clearly the possible inherent propagating waves. The drawback is that the energy distribution among the different components of the space harmonics and the different wave types is not readily given for a specific excitation. This is particularly the case for the periodic x-direction. Wave beaming plays a dominant role in some frequency bands, as expected already from the DFT results. For low frequencies global waves are prominent. With increasing frequency new wave types cut on, increasing the complexity of the wavenumber content. For profile C in particular, the distinct pass- and stop-band behaviour for bending wave propagation in the x-direction is obvious. Significant lateral wave propagation is possible only in the pass-bands 1500–2200 Hz and beyond 4200 Hz, see Figs. 10(d) and 5(a).

For propagation in the x- and z-direction the frequency dependent dispersion curves extracted are included in Fig. 5 for profile A, Fig. 6 for profile B and Fig. 7 for profile C with full lines. The dispersion curves for k_x agree, as expected, with the results of the two-dimensional investigation presented in Ref. [1].

The two-dimensional wave propagation results corroborate the included DFT results with much clearer pictures of the inherent possible waves. Moreover, the calculation and modelling effort is drastically reduced in comparison with the spatial Fourier transform approach as only one single periodic FE-subelement has to be modelled and calculated.

4. Dispersion characteristics using waveguide finite element technique

It is not directly possible to identify the wave shapes of the inherent waves in the profile from the full three-dimensional-FE-calculations or the phase constant surface results. These wave shapes are useful to gain insight into the wave propagation process. Moreover, full three-dimensional-modelling and FE-calculation of the light weight profiles is quite demanding with regard to computer resources and evaluation time. Therefore, a different approach is aimed at in order to investigate the wave propagation. In many applications, e.g. in train carriages the extension of the profiles along the carriage can be quite long, so that the structure-borne sound propagation is similar to an infinite extension in this direction whereas it is finite in the lateral direction.

The option is then to model only a cross section of the complete profile and to use WFE technique for the infinite extension in the z-direction. In contrast to the spectral finite element formulation introduced by Finnveden [19], there is no need to create new element types for the calculation. Standard FE-libraries and packages can be used to create the dynamic stiffness matrix of a cross section. This greatly enhances the applicability for general use so that complex geometries can be modelled easily.

4.1. Theory

The WFE approach models a section of the strip in the z-direction by conventional FE-methods using shell elements. An example of such a strip is shown in Fig. 19(b) which is investigated in Section 5.[2] This technique results in quite small FE-models as only a small part of a complete plate has to be modelled. For periodic strips in the x-direction it is sufficient to model only one subelement (see, e.g. Fig. 9). Extended sections in the x-direction can be assembled from these subelements by using standard FE-assembling methods. In

[2]In Ref. [1] the investigated strip is similar in shape, but in that case no extension in the z-direction is modelled and beam elements are used to calculate the wave propagation in the x-direction only.

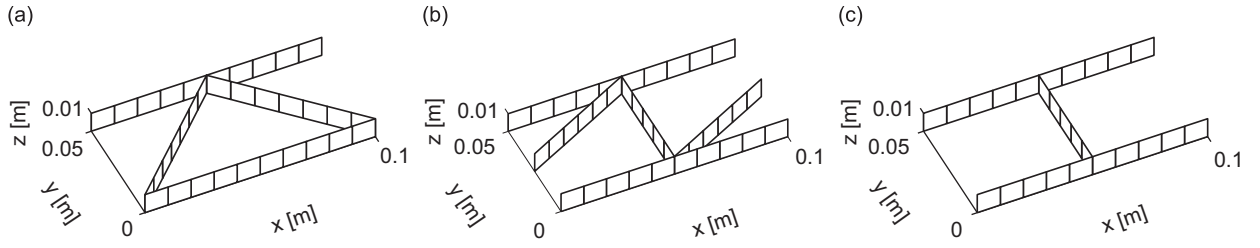

Fig. 9. FE-models of (a) profile A, (b) profile B and (c) profile C subelements, 10 mm element length.

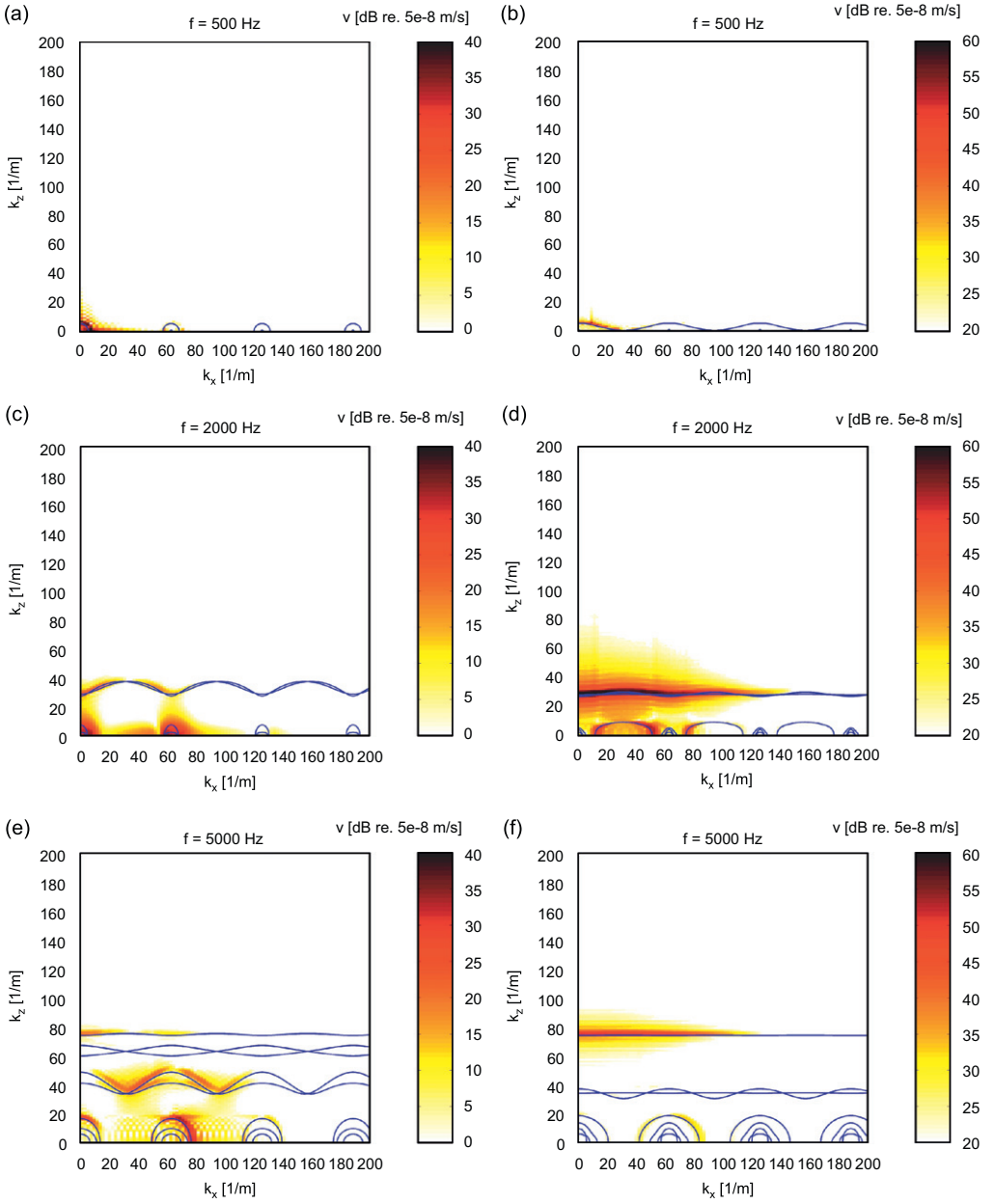

Fig. 10. Wavenumber content of profile A (a) 500 Hz, (c) 2000 Hz and (e) 5000 Hz and of profile C (b) 500 Hz, (d) 2000 Hz and (f) 5000 Hz (DFT results using colour shading and phase constant surface results with full dark lines).

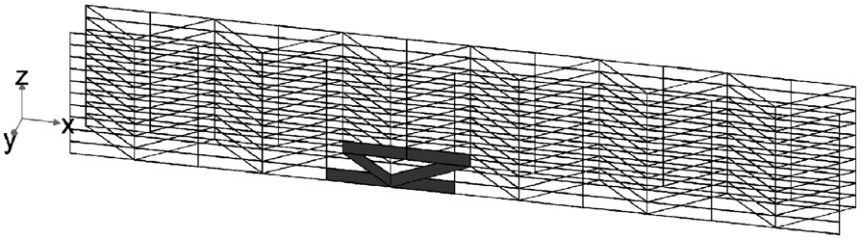

Fig. 11. Artificial periodic subelement (marked in black) as part of a complete light weight plate.

analogy to the case of multi-coupled periodic elements, it is assumed that this section is not only assembled in the x-direction, but repeated in the z-direction also to form an infinite plate in the latter direction (see Fig. 11).

Now the wave propagation in the z-direction can be investigated in analogy to multi-coupled periodic systems. Defining the edges of the section in the z-direction as the front and back end of the periodic element and assembling the transfer matrix offers the opportunity to solve the transfer matrix eigenvalue problem directly or based on the dynamic stiffness matrix. This approach has been used for rails to predict the wave propagation along the rail by calculating a small section of the rail, see, e.g. Refs. [20–22]. One problem for a complete profile strip is that a high number of coupling nodes is introduced enlarging the transfer matrix involved. In some cases the method can become unstable, but this instability can be circumvented by using appropriate FE-elements and a stable implementation to solve the eigenvalue problem. For details see, e.g. Refs. [23–25]. The same technique is also used for investigations of wave propagation in ultrasonics, e.g. Refs. [26,27].

The WFE-calculation is based on a standard FE-model of a subelement marked in black in Fig. 11 or a complete cross section model as shown in Fig. 19(b). Using the mass and stiffness matrices $\mathbf{M}$ and $\mathbf{S}$, the equation of motion for harmonic excitation using the time base $e^{j\omega t}$ and structural damping with loss factor η reads

$$(-\omega^2\mathbf{M} + (1 + j\eta)\mathbf{S})\boldsymbol{\xi} = \mathbf{F}. \tag{12}$$

The *dynamic* stiffness matrix $\mathbf{K}$ is defined and partitioned in the front (f) and back (b) dofs, see Fig. 8.[3]

$$\mathbf{K}\boldsymbol{\xi} = \begin{bmatrix} \mathbf{K}_{ff} & \mathbf{K}_{fb} \\ \mathbf{K}_{bf} & \mathbf{K}_{bb} \end{bmatrix} \begin{Bmatrix} \boldsymbol{\xi}_f \\ \boldsymbol{\xi}_b \end{Bmatrix} = \begin{Bmatrix} \mathbf{F}_f \\ \mathbf{F}_b \end{Bmatrix}. \tag{13}$$

A wave basis can be established based on the solution of the eigenvalue problem of the transfer matrix $\mathbf{T}$, relating the front and back edges of the subelement. The transfer matrix reads

$$\mathbf{T} \begin{Bmatrix} \boldsymbol{\xi}_f \\ \mathbf{F}_f \end{Bmatrix} = \begin{Bmatrix} \boldsymbol{\xi}_b \\ -\mathbf{F}_b \end{Bmatrix}. \tag{14}$$

The transfer matrix can be established from the partitioned dynamic stiffness matrix:

$$\mathbf{T} = \begin{bmatrix} -\mathbf{K}_{fb}^{-1}\mathbf{K}_{ff} & \mathbf{K}_{fb}^{-1} \\ -\mathbf{K}_{bf} + \mathbf{K}_{bb}\mathbf{K}_{fb}^{-1}\mathbf{K}_{ff} & -\mathbf{K}_{bb}\mathbf{K}_{fb}^{-1} \end{bmatrix}. \tag{15}$$

[3]For the applications used here no inner dofs are used in the subelement model so that the dynamic stiffness matrix contains only the front and back dofs. Otherwise the inner dofs have to be condensed.

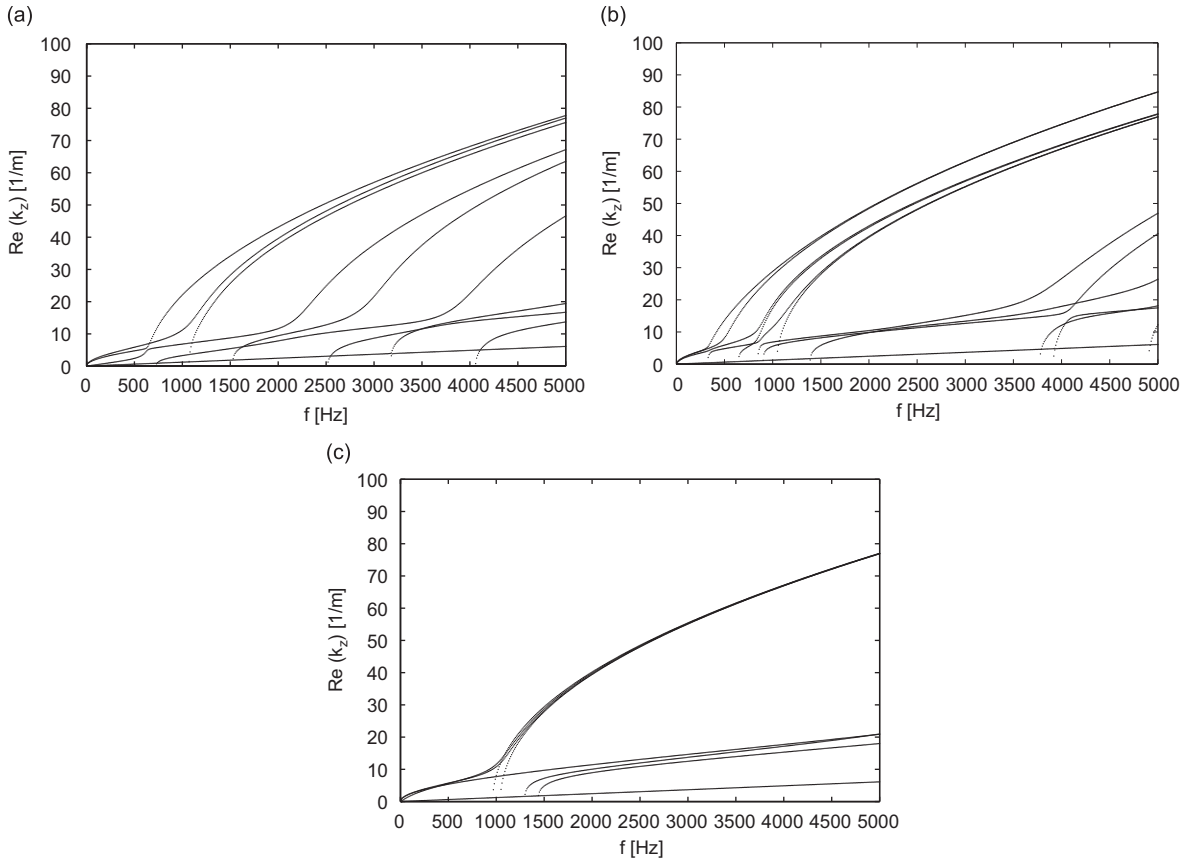

Fig. 12. Wavenumber content of single subelement in the z-direction (0.1 m width): (a) profile A, (b) profile B and (c) profile C.

Based on Bloch's theorem, relating the front and back edges of all the connected elements with a constant amplitude and phase shift λ, the eigenproblem for free wave propagation can be defined as

$$\mathbf{T}\begin{Bmatrix} \boldsymbol{\xi}_f \\ \mathbf{F}_f \end{Bmatrix} = \lambda \begin{Bmatrix} \boldsymbol{\xi}_f \\ \mathbf{F}_f \end{Bmatrix}, \quad \lambda = \mathrm{e}^{\mathrm{j}\, k_z L_e}. \tag{16}$$

Thence, the wavenumber k_z can be related directly to the eigenvalues λ with the periodic length L_e in the z-direction. In undamped systems the waves are either purely propagating ($|\lambda| = 1$), decaying ($\mathrm{Im}(\lambda) = 0$), or complex for all remaining λ. Though the mathematical solution is ambiguous with a periodicity of $2\pi/L_e$ for the real part of the wavenumber, a distinct identification, in this case in z-direction, is possible in contrast to most typical periodic systems. Assuring a high wavenumber periodicity length by selecting a very small periodic length L_e, the solution for lowest wavenumbers gives the physical results. For accurate results, the periodic length has to be much smaller than any occurring physical wavelength, $k_z L_e < 1$. This criterion is in accordance with standard FE-modelling guidelines where six elements per wavelength is a common rule of the thumb. As pointed out by Mead in [28] a selection of a small L_e increases the accuracy without increasing calculation time as the dimensions of the eigenproblem to solve are independent of this choice. This implies a significant advantage over standard FE-modelling techniques.[4]

[4]The selection of a small L_e is bounded by numerical issues, resulting, e.g. from round-off errors in the corresponding matrices for very small elements [25].

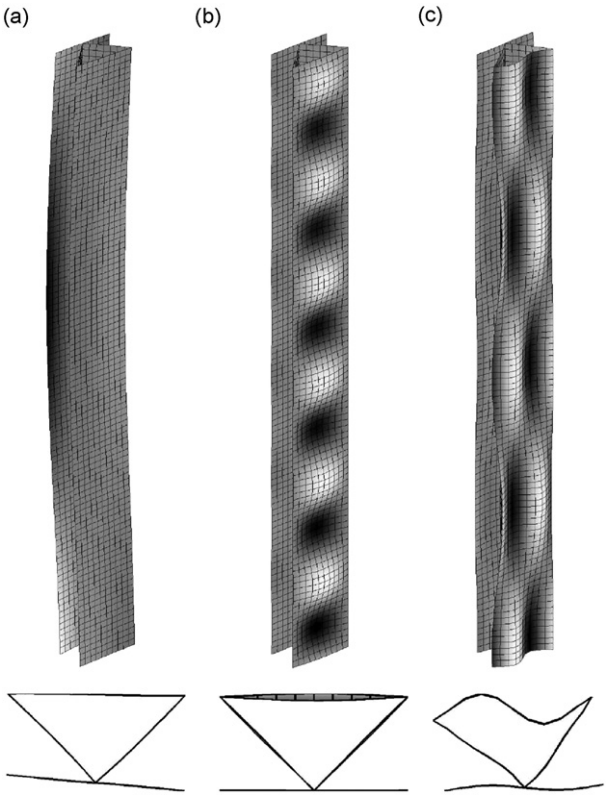

Fig. 13. Selected wave shapes of single subelement profile A. (a) $k_z = 4.7\,\mathrm{m}^{-1}$, $f = 500\,\mathrm{Hz}$; (b) $k_z = 37.7\,\mathrm{m}^{-1}$, $f = 2000\,\mathrm{Hz}$ and (c) $k_z = 13.6\,\mathrm{m}^{-1}$, $f = 5000\,\mathrm{Hz}$. Cross sectional plots (x–y) are included at the bottom for $z = 0$.

The wave basis is constituted by the pairs of negative and positive travelling waves with the eigenvalues λ_i and the corresponding right eigenvectors as defined in Eq. (16), $\boldsymbol{\phi}_i = [\boldsymbol{\xi}_{f,i}\mathbf{F}_{f,i}]^{\mathrm{T}}$, which define the wave shapes. These wave vectors can be assembled in an eigenvector matrix $\boldsymbol{\Phi}$.

4.2. Wave propagation in single subelement profiles

To gain insight in the principal wave propagation features of the generic light weight profiles the different subelements are investigated with free boundary conditions at the left and right edge at first, forming profiles of single subelements in the x-direction.

The dispersion characteristics of the three configurations are extracted from the FE-models shown in Fig. 9, using shell elements with an element length of 10 mm.

All six dof at each node including the in-plane rotations are used in the extraction procedure.[5]

The propagating waves are identified by using a limit for λ, typically $0.99 < |\lambda| \leqslant 1$. The real part of these wavenumbers is plotted in Fig. 12 for subelements A–C.

In the low frequency regime up to about 600 Hz for profile A global waves with wavenumber up to $8\,\mathrm{m}^{-1}$ are present. A typical wave shape is shown for profile A in Fig. 13(a) for 500 Hz. For higher frequencies wave propagation in the member plates cuts on and wave shapes with these local vibration patterns are shown for 2000 and 5000 Hz. The shading indicates the displacement in the y-direction.

[5]CQUADR shell elements are used for a stable wavenumber extraction. In contrast to the CQUAD4 elements, these elements include the in-plane rotational dof. This is important to represent the waves in the diagonal stiffeners correctly, where a portion is in-plane also [29].

For profile B local wave propagation starts already at 300 Hz. This is related to the special layout of the subelement with three free plate edges on both lateral edges. The corresponding wave shapes are plotted in Fig. 14.

For profile C some characteristic waves are shown in Fig. 15. The wavenumber content comprises less branches which can be explained by four similar plate fields concentrating to the same bending wavenumbers.

All the profiles show a global bending branch which continues at high frequencies and the non-dispersive longitudinal wave branch with low wavenumbers, reaching a wavenumber of about $7\,\mathrm{m}^{-1}$ at 5000 Hz.

4.3. Wave propagation in multiple subelement profiles

The dispersion investigation of a single free subelement profile is not representative for industrial applications where a full plate consists of several adjacent subelements. Hence, it is necessary to investigate the influence of building a complete profile of the subelements. In order to get an idea of the general trends, a calculation with five subelements side by side is performed. The resulting dispersion characteristics for five subelements are shown in Fig. 16.

Comparing the dispersion plots for one and five subelements, it is obvious that the number of propagating waves increases with the plate width. Despite the diversity of waves it is possible to distinguish different local wave groups that can be found in the dispersion plots irrespective of plate width. Exemplified for profile A the following observations can be made:

- The dispersion curve with the highest wavenumber is related to edge waves of the cantilevered sections. Because of the free edges these are the first local waves to cut on (see Fig. 17(a)).

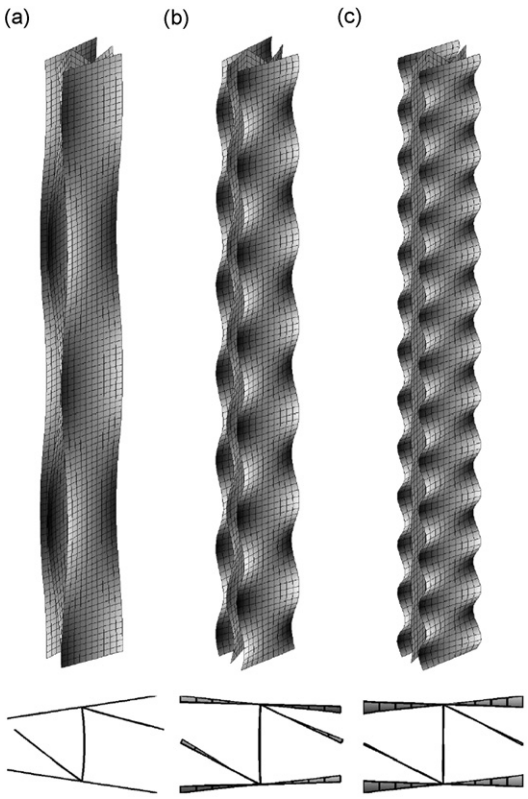

Fig. 14. Selected wave shapes of single subelement profile B. (a) $k_z = 13.6\,\mathrm{m}^{-1}$, $f = 500\,\mathrm{Hz}$; (b) $k_z = 42.9\,\mathrm{m}^{-1}$, $f = 2000\,\mathrm{Hz}$ and (c) $k_z = 77.7\,\mathrm{m}^{-1}$, $f = 5000\,\mathrm{Hz}$. Cross sectional plots (x–y) are included at the bottom for $z = 0$.

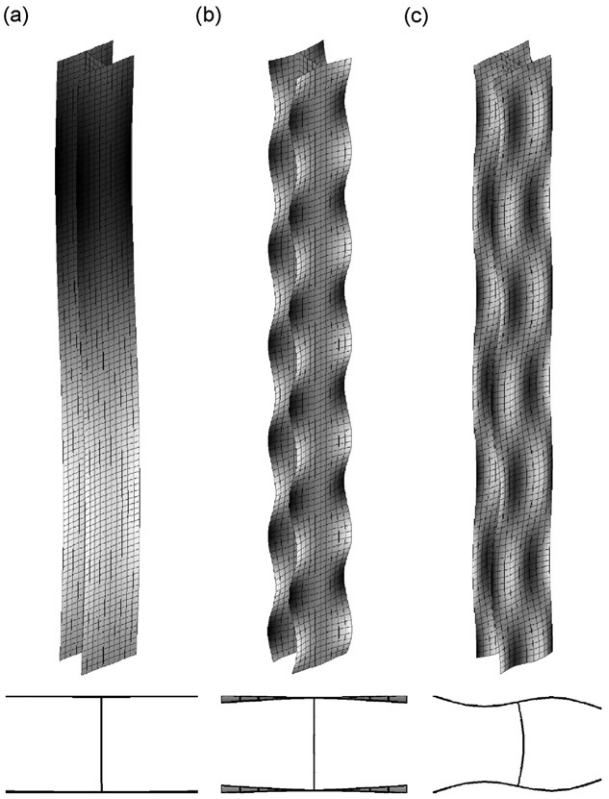

Fig. 15. Selected wave shapes of single subelement profile C. (a) $k_z = 5.7\,\mathrm{m}^{-1}$, $f = 500\,\mathrm{Hz}$; (b) $k_z = 39.4\,\mathrm{m}^{-1}$, $f = 2000\,\mathrm{Hz}$ and (c) $k_z = 20.8\,\mathrm{m}^{-1}$, $f = 5000\,\mathrm{Hz}$. Cross sectional plots (x–y) are included at the bottom for $z = 0$.

- The second group is related to waves comprising first-order mode shapes of the plate strip members. For the waves with the highest wavenumbers in this group, adjacent plate strips vibrate in anti-phase (simply supported mode shape, Fig. 17(b)), whereas for the lower wavenumbers they vibrate in-phase (clamped mode shape, Fig. 17(c)). This behaviour is similar to the characteristic wave shapes of a simply supported periodic beam [30, p. 186]. For a fixed wavenumber the region between these extremes can be regarded as a wave pass-band with the bounding frequencies of the plate strip with either simply supported or fixed edges.
- The third group ($k = 60-67\,\mathrm{m}^{-1}$ for 5000 Hz) is dominated by vibrations of the intermediate inclined webs in the first cross mode (see Fig. 17(d)).
- The fourth group ($k = 35-48\,\mathrm{m}^{-1}$ for 5000 Hz) is characterized by second-order cross modes of the outer plate strips. Again the high wavenumber limit of this group corresponds to simply supported vibrations of the members (Fig. 17(e)) and the lower edge is related to clamped motion, not shown for the sake of brevity.
- In the low wavenumber range ($k = 5-17\,\mathrm{m}^{-1}$ for 5000 Hz) the waves comprise mainly rotational behaviour at the joints (Fig. 17(f)).
- Oblique directional wave propagation can be observed for the upper edges of the wave groups (Fig. 17(b) and (e)).

Similar observations for infinite periodically-stiffened plates are reported by Mace [31], where the bounding frequencies of the propagation zones are shown to be linked to distinct propagation constants of $\mu = 0$ and π in the lateral direction (in-phase and out-of phase motion of adjacent bays). Similar wave groups for extruded profile floor sections are also identified from spectral finite element investigations [32], but are not linked to the investigated strip width.

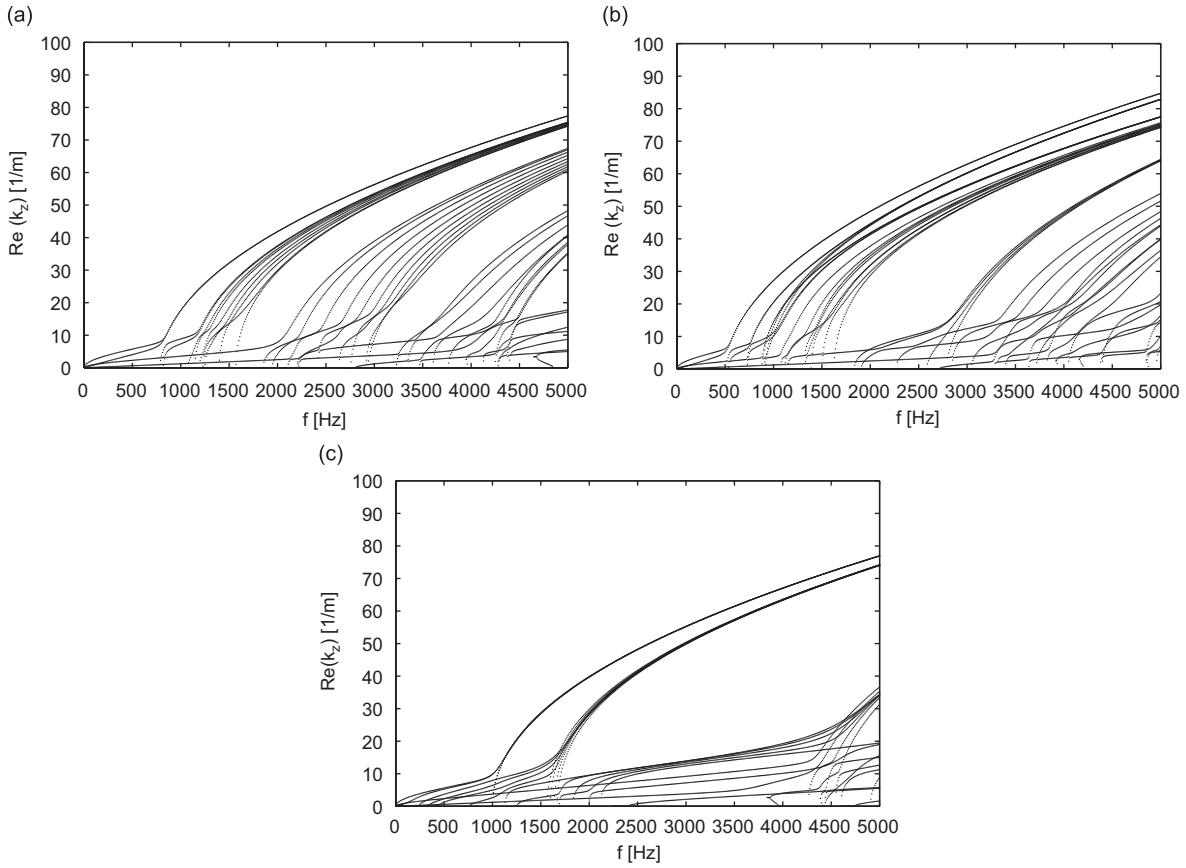

Fig. 16. Wavenumber content in the z-direction of five subelements (0.5 m width): (a) profile A, (b) profile B and (c) profile C.

The general observation of wave groups holds also for profile B. Wave shapes are omitted for profile B for the sake of brevity.

The wave groups for profile C are even clearer as the coupling between different wave types is more distinct than for profiles with inclined webs due to the right-angled web connections. Some typical wave shapes are plotted in Fig. 18. Global wave motion as shown in Fig. 18(a) in the lateral direction is characterized by significantly smaller wavelengths for a profile without inclined webs, corroborating the DFT and phase constant surface results. This is related to an increased number of global waves cutting on in the low frequency range for a plate width of 0.5 m. The local waves show similar trends as described previously for profile A.

5. Application example: regional train floor section

In this section dispersion characteristics of a regional train floor section are investigated. Since this plate is not strictly periodic in the lateral direction, the extraction of the dispersion characteristics using phase constant surfaces is not an option. Hence, the WFE technique and the spatial Fourier transformation of standard FE results are applied. For experimental validation, dispersion characteristics are extracted using the IWC technique.

The light weight train floor section made of extruded aluminium sections which are line-welded in the longitudinal z-direction is shown in Fig. 19(a).

The detailed geometry is not given here for the sake of brevity, but the plate thicknesses are 2.5−3 mm, overall thickness is 60 mm and the main spacing between adjacent webs is about 180 mm. This structure is not strictly periodic and it has some outer ribs for inner floor and equipment fastening which are neglected in the simulations.

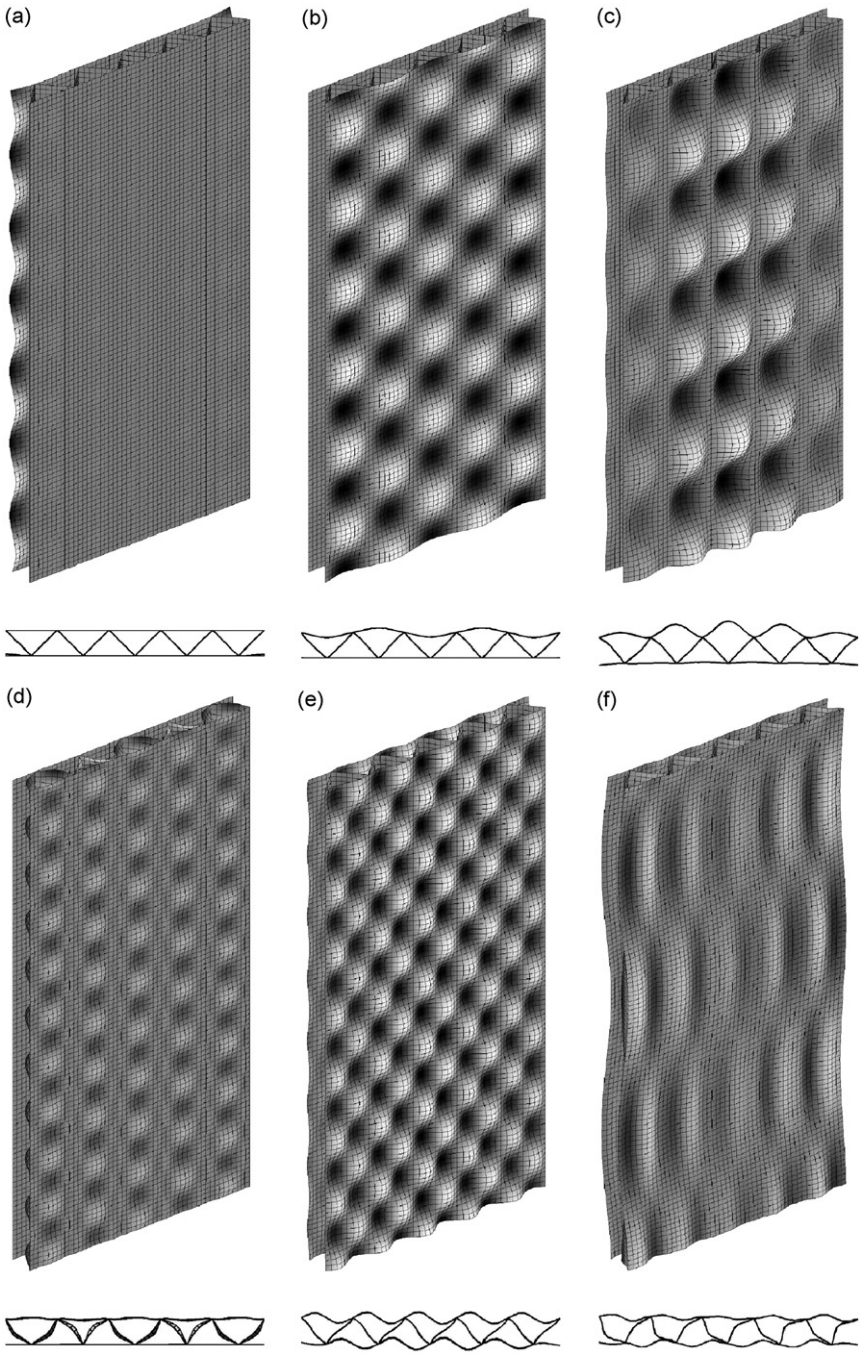

Fig. 17. Selected wave shapes for profile A (0.5 m width). (a) $k_z = 41.9\,\mathrm{m}^{-1}$, $f = 2000\,\mathrm{Hz}$; (b) $k_z = 37.5\,\mathrm{m}^{-1}$, $f = 2000\,\mathrm{Hz}$; (c) $k_z = 30.0\,\mathrm{m}^{-1}$, $f = 2000\,\mathrm{Hz}$; (d) $k_z = 63.3\,\mathrm{m}^{-1}$, $f = 5000\,\mathrm{Hz}$; (e) $k_z = 48.3\,\mathrm{m}^{-1}$, $f = 5000\,\mathrm{Hz}$ and (f) $k_z = 11.2\,\mathrm{m}^{-1}$, $f = 5000\,\mathrm{Hz}$. Cross sectional plots (x–y) are included at the bottom for $z = 0$.

The FE-modelled half cross section is shown in Fig. 19(b). As the forced response for excitation in the y-direction at the centre of the plate is investigated here, only the half cross section is modelled and symmetric boundary conditions are applied at the edge $x = 1.2\,\mathrm{m}$. The edge ($x = 0-0.4\,\mathrm{m}$) is highly damped with a loss

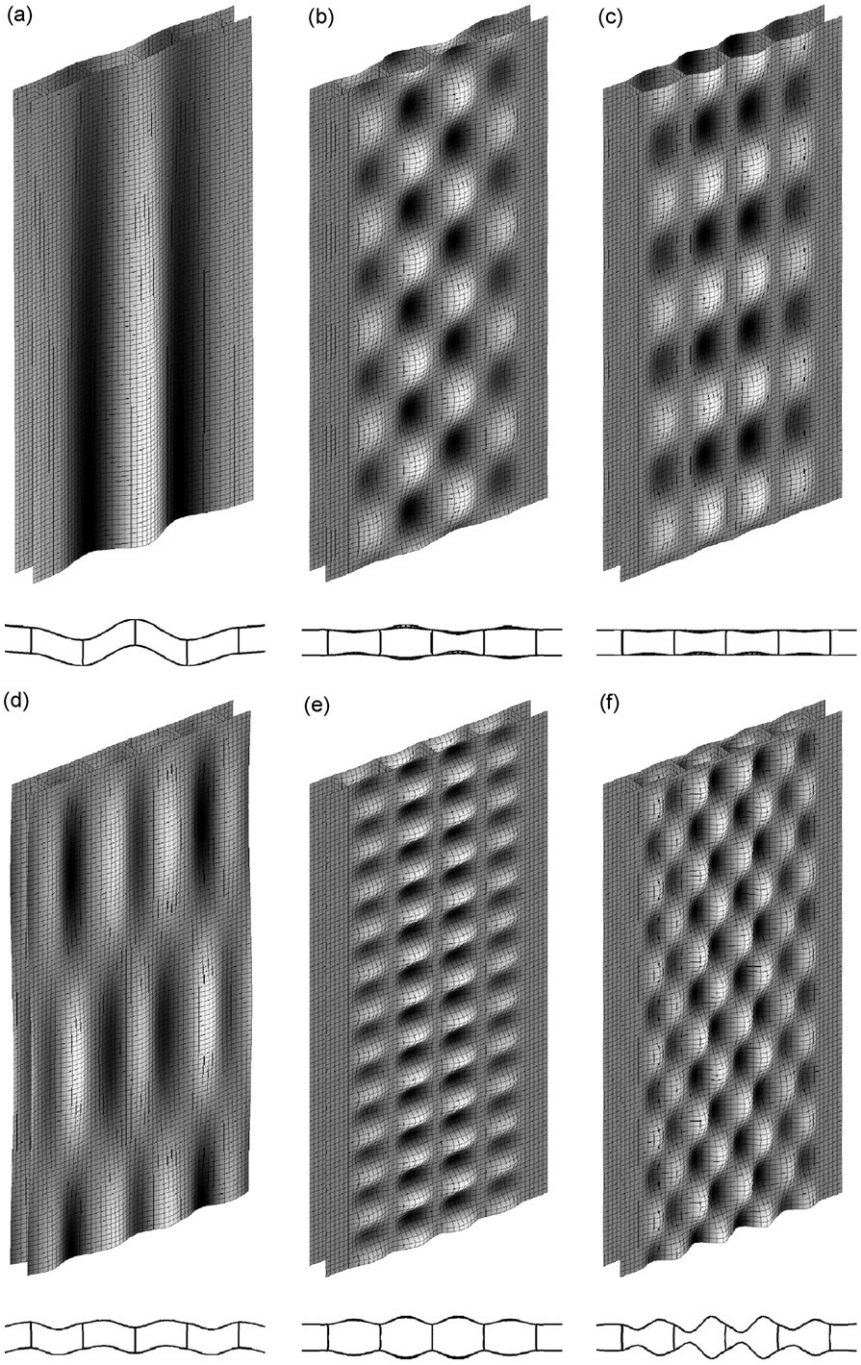

Fig. 18. Selected wave shapes for profile C (0.5 m width). (a) $k = 1.2\,\mathrm{m}^{-1}$, $f = 500\,\mathrm{Hz}$; (b) $k_z = 29.8\,\mathrm{m}^{-1}$, $f = 2000\,\mathrm{Hz}$; (c) $k_z = 27.4\,\mathrm{m}^{-1}$, $f = 2000\,\mathrm{Hz}$; (d) $k_z = 7.8\,\mathrm{m}^{-1}$, $f = 2000\,\mathrm{Hz}$; (e) $k_z = 74.0\,\mathrm{m}^{-1}$, $f = 5000\,\mathrm{Hz}$ and (f) $k_z = 36.7\,\mathrm{m}^{-1}$, $f = 5000\,\mathrm{Hz}$. Cross sectional plots (x–y) are included at the bottom for $z = 0$.

factor of $\eta = 0.1$ to reduce edge reflections. This simulates test conditions, where the edge is embedded in sand and partially filled with foam wedges and sand to establish a smooth transition to the damped regions, see Ref. [33] for details of the experimental set-up.

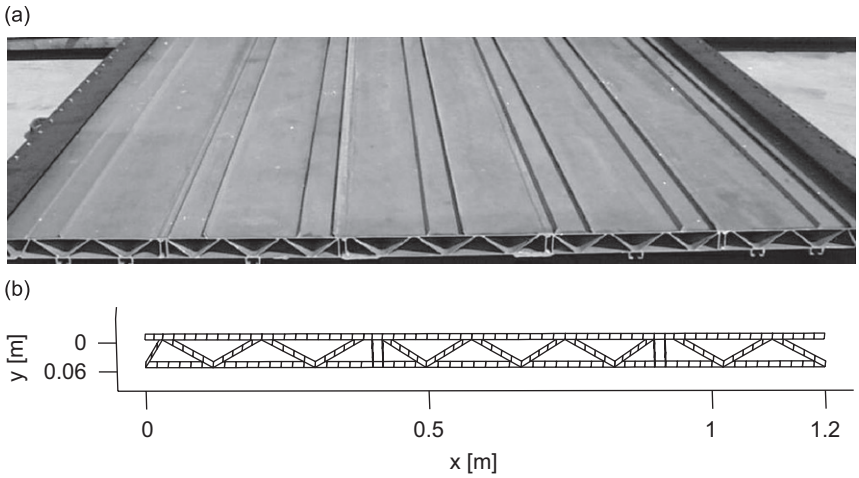

Fig. 19. Light weight train floor section (extruded aluminium). (a) Photo (b) WFE model of half cross section, 20 mm element length in the z-direction.

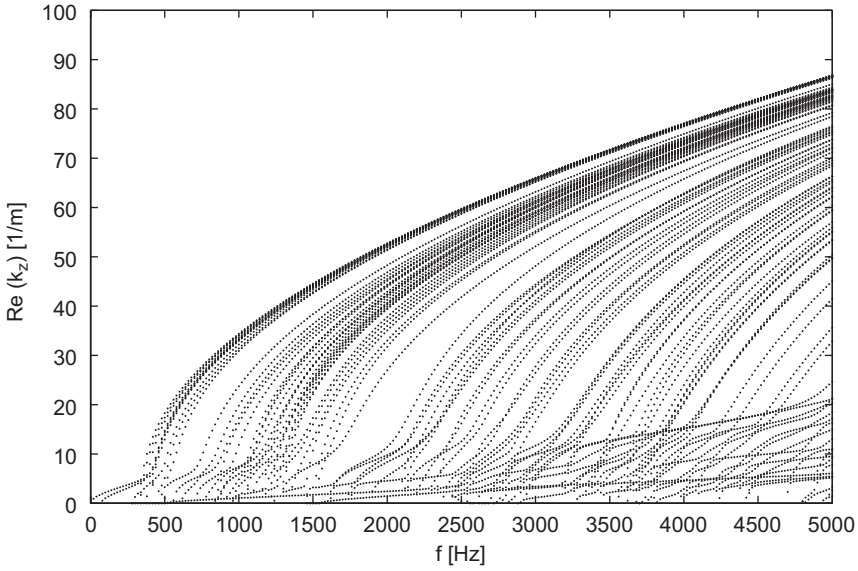

Fig. 20. Dispersion characteristics of propagating waves in light weight train floor with symmetric boundary conditions and infinite extension in the z-direction using WFE approach.

5.1. Calculated dispersion characteristics

The dispersion characteristics extracted from the WFE eigenvalue problem for symmetric waves of the plate are shown in Fig. 20.[6]

Because of the irregularity of the cross section, the wave dispersion is less distinct than for the ideal generic profiles investigated before. However, similar general trends can be observed. Solely global bending waves propagate at frequencies up to 300 Hz. At higher frequencies, again, different wave groups develop. For

[6]Only symmetric waves are included because of the symmetric boundary condition applied. This solution is sufficient to investigate the case of symmetric excitation in the centre position.

4000 Hz, where most of the types have cut on, some wave shapes are plotted in Fig. 21 as examples of each wavegroup.

The group with highest wavenumbers in Fig. 20 at 4000 Hz is related to first-order cross modes of the outer plate strips (see Fig. 21(a)). These local waves are the first to cut on in frequency because of the highest distance between adjacent web joints. The second dispersion group of Fig. 20 is dominated by first-order cross modes of the interior diagonal plates (see Fig. 21(b)). The amplitudes of the outer plates for this group are significantly lower than for the inner webs.

For all the waves with high wavenumbers in the z-direction, the vibrating region in the x-direction is bounded and the different waves in each group belong to different vibrating regions in the x-direction. The straight intermediate webs exhibit a strong barrier for the wave motion which is passed only by the waves with a low wavenumber in the z-direction (Figs. 21(h) and (i)).

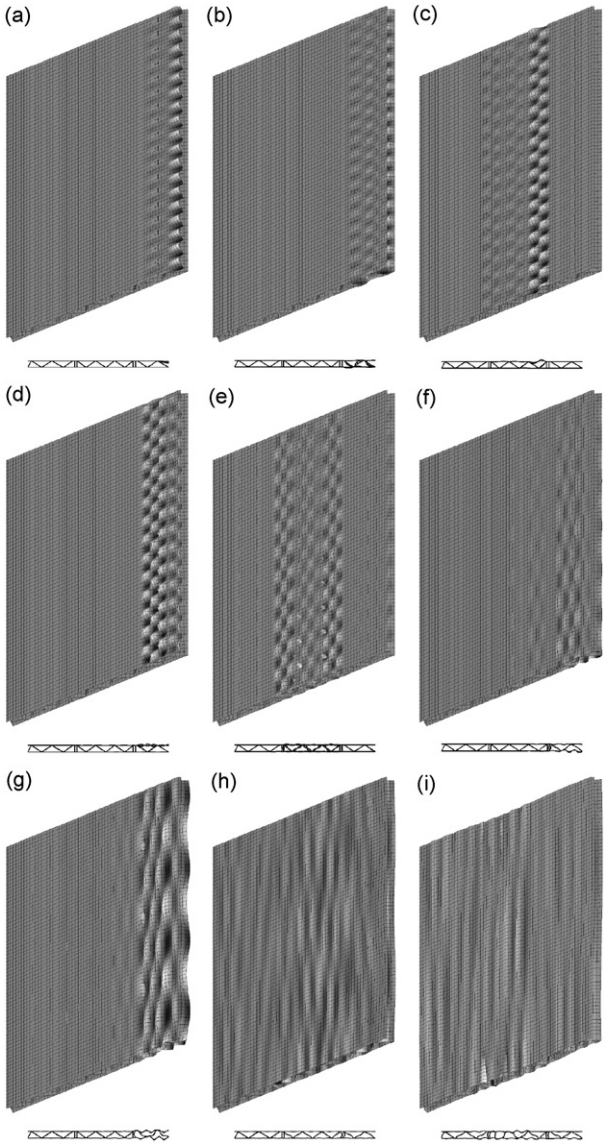

Fig. 21. Selected wave shapes for half train floor plate with symmetric boundary conditions, $f = 4000$ Hz. (a) $k_z = 77.0\,\mathrm{m}^{-1}$, (b) $k_z = 73.9\,\mathrm{m}^{-1}$, (c) $k_z = 69.2\,\mathrm{m}^{-1}$, (d) $k_z = 59.2\,\mathrm{m}^{-1}$, (e) $k_z = 44.7\,\mathrm{m}^{-1}$, (f) $k_z = 24.7\,\mathrm{m}^{-1}$, (g) $k_z = 15.2\,\mathrm{m}^{-1}$, (h) $k_z = 8.0\,\mathrm{m}^{-1}$ and (i) $k_z = 3.7\,\mathrm{m}^{-1}$. Cross sectional plots (x–y) are included at the bottom for $z = 0$.

The wavegroups with lower wavenumbers than $60\,m^{-1}$ at 4000 Hz are not as distinct as the first-order modes previously described since different wavegroups overlap.

Figs. 21(c) and (d) show examples of second- and third-order cross modes of the outer plate strips, respectively. Fig. 21(e) is a combination of third-order outer plate strip and second-order diagonal plate strip modes, whereas Fig. 21(f) is a mixture of fourth-order outer plate and first-order straight inner web modes.

Some waves with global z-behaviour are shown in Figs. 21(g)–(i), where the last two waves comprise wave motion extended over the complete profile width.

From the nature of the characteristic wave shapes some important aspects of structure-borne sound propagation in the light weight profile at frequencies beyond the global wave region can be deduced:

- For local excitation of structures which are not strictly periodic, bounded wave motion is expected in the section of excitation with power flow mainly in the z-direction.
- Irregularities such as heavy straight webs behave as wave "blockers".
- Extended lateral vibration of the plate is likely to be connected to global wave motion in the z-direction.
- Damping is acting locally in the region of the damped plate strips. The edge damping applied in the example has very little effect on the characteristic waves propagating in the central region of the plate.
- The cut-on frequencies for cross modes in the plate strips are somewhere between the lateral eigenfrequencies of simply supported and clamped plate strips. The low frequency edge of the wavegroup corresponds roughly to the simply supported case, whereas the high frequency edge belongs to the clamped case. This is in accordance with the observed wave shapes for the ideal periodic profiles investigated. The variety of boundary conditions is achieved by different combinations of displacement patterns of adjacent connected plate strips. For narrow light weight plates the amount of variations is limited which causes a reduced set of emerging boundary conditions and related characteristic waves. For wider plates the number of characteristic waves increases significantly as illustrated for the regional train floor example.

5.2. Measured dispersion characteristics

The measured velocity field of the plate is used to extract its dispersion characteristics. The limited test area hampers the application of the spatial Fourier transform previously used for wavenumber extraction from calculated response fields. In order to improve the resolution and the applicability for arbitrary test positions the IWC method is applied [9,12].

For each frequency, dispersion characteristics in the k_x–k_z domain can be extracted. As an example the results for 1000 Hz are shown in Fig. 22.[7] Results for other frequencies are omitted for the sake of brevity. The strong wave guiding along the plate strip is obvious in the calculated and measured results of Fig. 22 with a dominant dispersion line parallel to the k_x-axis. The frequency shift due to the stiffening effect of the fillets at the plate joints identified and reported in Ref. [1] is now manifested by a wavenumber shift for k_z. The stiffening effect speeds up the bending wave and reduces the wavenumbers.

Evaluated frequency dependent measured dispersion characteristics in the x- and z-direction are shown in Fig. 23. In order to increase legibility the correlation values are normalized by the maximum value at each frequency.

Dispersion characteristics extracted using the spatial Fourier transform approach of the force excited plate are shown in Fig. 24 for comparison.

In general, wave propagation in the x-direction is not so distinct as in the z-direction. In the low frequency range, global wave propagation with similar wavenumbers in both directions exists. For higher frequencies waves with first-order cross modes dominate the propagation along the plate strips corroborating the insights gained from the WFE investigations. A slight periodicity of the wavenumbers in the x-direction can be observed as expected for nearly periodic systems. Faint decreasing dispersion lines, related to reflected waves, are also detectable for calculated and measured results.

[7]Due to different evaluation techniques (DFT and IWC) a direct quantitative comparison of the results is not possible. Interpretation should be based on pattern recognition.

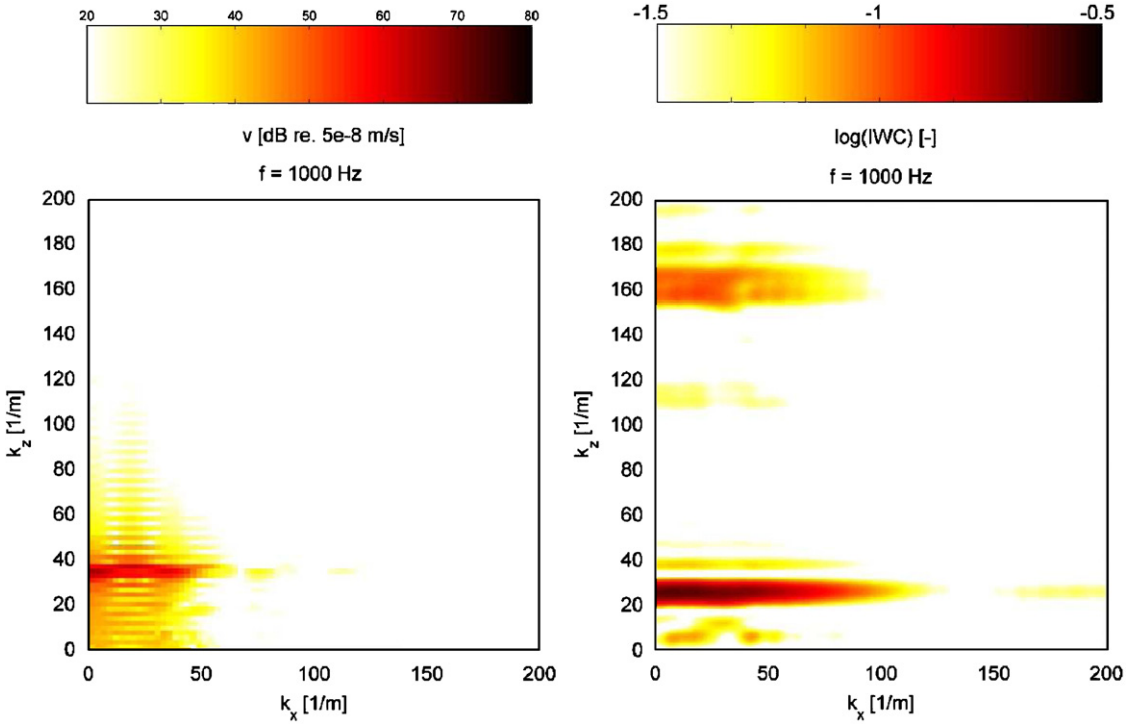

Fig. 22. DFT-calculated (left) and IWC-measured (right) dispersion characteristics of regional train floor section, $f = 1000$ Hz, F_y at the centre of plate field.

Dispersion in the z-direction can be compared also with WFE-results of Fig. 20 and show a high degree of similarity for both calculation results. The measured dispersion follows the WFE-dispersion characteristics with highest wavenumbers which are strongly excited. All other WFE dispersion branches with lower wavenumbers are not excited in the measurement set-up with normal force excitation at the centre of a plate field.

6. Concluding remarks

The dispersion characteristics of light weight plates with truss-like core geometries demonstrates that wave beaming is not only limited to structures with periodicity in both directions, but arises also for structures comprising periodicity only in one direction. The strong periodic effects identified from the two-dimensional investigation in Ref. [1] are evident in the three-dimensional plate investigation in the corresponding periodic direction. In contrast to the strip investigation, where power transmission and wave propagation is nearly completely suppressed in the stop-bands, the effect is reduced for the plates investigated. In the lateral stop-bands wave propagation in the z-direction is still enabled and wave spreading in oblique directions depends on the geometric profile layout, which influences the coupling mechanisms and wave conversions at the joints. For profiles with inclined webs distinct wave beaming in oblique directions arise, whereas for a profile with straight webs lateral coupling and oblique propagation is reduced. The frequency dependent stop-band behaviour for one-dimensional wave propagation is ''transformed'' into a frequency dependent and spatially varying attenuation for the two-dimensional propagation case, establishing low vibration regions for point excited structures. The weakened stop-band effect makes general applications for noise control somewhat delicate. In special situations where low vibration is requested especially in certain regions, e.g. for installation of vibrational sensitive equipment, this strong wave beaming might be exploited. Moreover, design of damping treatments can be optimized, at least for point excited structures, by exploiting the wave beaming effects and aligning the damping treatments in the beaming directions from the point of excitation.

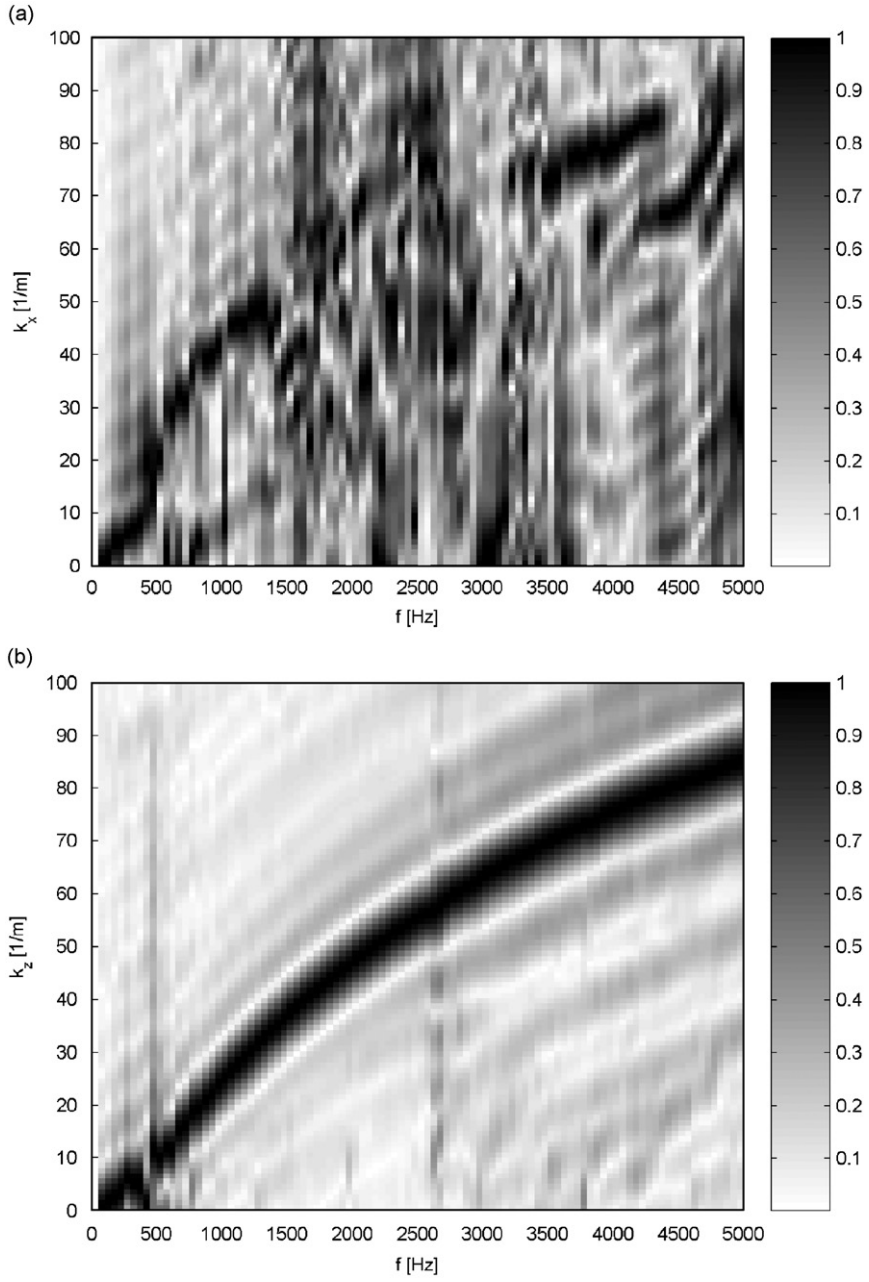

Fig. 23. Measured dispersion characteristics using IWC method in (a) the x- and (b) the z-direction, normalized by the maximum of each frequency, F_y at the centre of plate field.

From a structural acoustic point of view it is vital to differentiate between subsonic and supersonic waves in the light weight plates. The dispersion characteristics presented establish a basis for their discrimination. Only the supersonic waves can couple efficiently to the ambient fluid. This is of major importance for radiation and transmission investigations. For proper acoustic design it could be valuable to investigate where major structural wave components become supersonic. In this respect the significant components of the space harmonic series in the periodic direction have to be included as it seems to be possible that low supersonic orders play a dominant role for radiation and transmission.

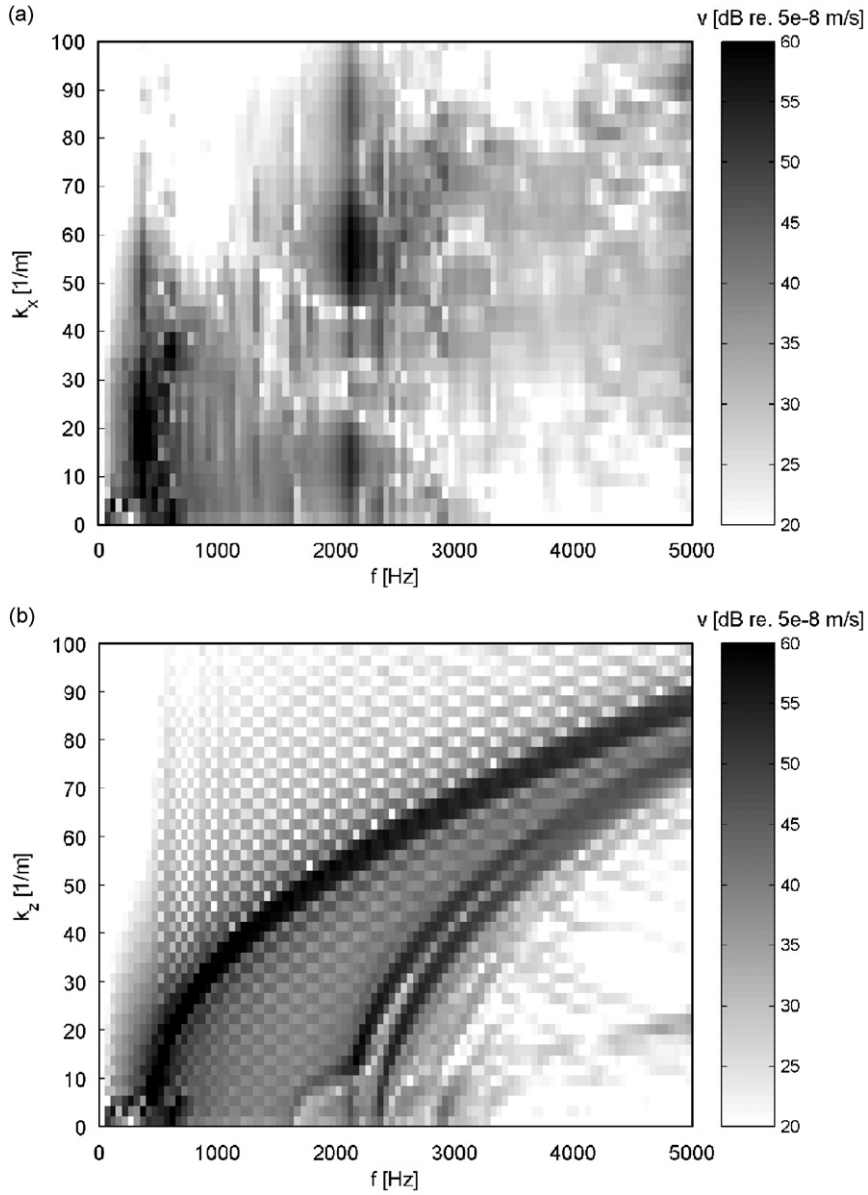

Fig. 24. Calculated dispersion of train floor section in (a) the x- and (b) the z-direction using the spatial Fourier transform of standard FE-results, F_y at the centre of plate field.

The regional train floor example demonstrates the applicability of the waveguide finite element method for free wave propagation on real extruded profile plates. It is demonstrated by validation measurements on dispersion that the salient physical behaviour is adequately described by the calculation model. An improved model could be established if the outer webs of the real floor would be included. This is in principle possible by extending the WFE cross section model in this respect. Moreover, the stiffening effect of the fillets at the joints should be included to improve accuracy of the models, e.g. by increasing the shell element thickness at the joints.

The WFE investigation of wave propagation reveals some interesting aspects for profile design. For structures which show a significant aperiodicity, bounded wave motion is expected in the directly excited section with power flow mainly in the direction parallel to the webs. Strong irregularities, e.g. a pair of straight

webs, mainly arising at weld junctions can behave as wave blockers in lateral direction. Damping is expected to act locally in the region of the damped plate strip. This observation can be used for efficient damping layer layout, if local structure-borne excitation is of concern.

Acknowledgements

The funding of the German Research Foundation (DFG) within the project "Körperschall typischer Leichtbaustrukturen" (Pe 1155/3) is gratefully acknowledged. Many thanks to the diligent experimental support of Carsten Hoever to extract the dispersion characteristics.

References

[1] T. Kohrs, B.A.T. Petersson, Wave propagation in light weight profiles with truss-like cores: wavenumber content, forced response and influence of periodicity perturbations, *Journal of Sound and Vibration* 304 (3–5) (2007) 691–721.
[2] R.S. Langley, N.S. Bardell, The response of two-dimensional periodic structures to harmonic point loading: a theoretical and experimental study of a beam grillage, *Journal of Sound and Vibration* 207 (4) (1997) 521–535.
[3] M. Ruzzene, P. Tsopelas, Control of wave propagation in sandwich plate rows with periodic honeycomb core, *Journal of Engineering Mechanics* 129 (9) (2003) 975–986.
[4] D. Duhamel, B.R. Mace, M.J. Brennan, Finite element analysis of the vibrations of waveguides and periodic structures, *Journal of Sound and Vibration* 294 (1–2) (2006) 205–220.
[5] B.R. Mace, D. Duhamel, M.J. Brennan, L. Hinke, Finite element prediction of wave motion in structural waveguides, *Journal of the Acoustical Society of America* 117 (5) (2005) 2835–2843.
[6] K. Grosh, E.G. Williams, Complex wave-number decomposition of structural vibrations, *Journal of the Acoustical Society of America* 93 (2) (1993) 836–848.
[7] J.G. McDaniel, W.S. Shepard Jr., Estimation of structural wave numbers from spatially sparse response measurements, *Journal of the Acoustical Society of America* 108 (4) (2000) 1674–1682.
[8] P.J. Halliday, K. Grosh, Maximum likelihood estimation of structural wave components from noisy data, *Journal of the Acoustical Society of America* 111 (4) (2002) 1709–1717.
[9] J. Berthaut, M.N. Ichchou, L. Jezequel, K-space identification of apparent structural behaviour, *Journal of Sound and Vibration* 280 (2005) 1125–1131.
[10] N.S. Ferguson, C.R. Halkyard, B.R. Mace, K.H. Heron, The estimation of wavenumbers in two-dimensional structures, *Proceedings of ISMA 2002*, Leuven, 2002.
[11] C.R. Halkyard, Maximum likelihood estimation of flexural wavenumbers in lightly damped plates, *Journal of Sound and Vibration* 300 (2007) 217–240.
[12] O. Bareille, M. Ichchou, J. Berthaut, L. Jezequel, Numerical extraction of dispersion curves from experimental data, *NOVEM 2005*, St. Raphael, France, 2005.
[13] C.M. Nilsson, C. Jones, A coupled waveguide finite and boundary element method for calculating the sound transmission through complex panel structures, in: Michael J Brennan (Ed.), *IX International Conference on Recent Advances in Structural Dynamics*, Institute of Sound and Vibration Research, University of Southampton, Southampton, UK, 2006.
[14] T. Kohrs, Structural-acoustic Investigation of Orthotropic Plates, Master's Thesis, Technische Universität Berlin, Institut für Technische Akustik, 2002.
[15] T. Kohrs, B.A.T. Petersson, Wave guiding effects in light weight plates with truss-like core geometries, *19th International Congress on Acoustics*, Madrid, 2–7 September 2007.
[16] R.S. Langley, The response of two-dimensional periodic structures to point harmonic forcing, *Journal of Sound and Vibration* 197 (4) (1996) 447–469.
[17] D.J. Mead, D.C. Zhu, N.S. Bardell, Free vibration of an orthogonally stiffened flat plate, *Journal of Sound and Vibration* 127 (1) (1988) 19–48.
[18] S.M. Jeong, M. Ruzzene, Analysis of vibration and wave propagation in cylindrical grid-like structures, *Shock and Vibration* 11 (2004) 311–331.
[19] S. Finnveden, Exact spectral finite element analysis of stationary vibrations in a railway car structure, *Acta Acustica* 2 (1994) 461–482.
[20] D.J. Thompson, Wheel-rail noise generation, III: rail vibration, *Journal of Sound and Vibration* 161 (3) (1993) 421–446.
[21] J. Gomez, E.G. Vadillo, J. Santamaria, A comprehensive track model for the improvement of corrugation models, *Journal of Sound and Vibration* 293 (2006) 522–534.
[22] I. Bartoli, A. Marzani, L. Lanza di Scalea, E. Viola, Modeling wave propagation in damped waveguides of arbitrary cross-section, *Journal of Sound and Vibration* 295 (2006) 586–707.
[23] W.X. Zhong, F.W. Williams, On the direct solution of wave propagation for repetitive structures, *Journal of Sound and Vibration* 181 (3) (1995) 485–501.
[24] L. Houillon, M.N. Ichchou, L. Jezequel, Wave motion in thin-walled structures, *Journal of Sound and Vibration* 281 (2005) 483–507.

[25] Y. Waki, B.R. Mace, M.J. Brennan, On numerical issues for the wave/finite element method, Technical Memorandum No. 964, Institute of Sound and Vibration Research, University of Southampton, December 2006.
[26] T. Hayashi, W.-J. Song, J.L. Rose, Guided wave dispersion curves for a bar with an arbitrary cross-section, a rod and a rail example, *Ultrasonics* 41 (2003) 175–183.
[27] T. Hayashi, C. Tamayama, M. Murase, Wave structure analysis of guided waves in a bar with an arbitrary cross-section, *Ultrasonics* 44 (2006) 17–24.
[28] D.J. Mead, An introduction to FE-PST the combined use of finite element analysis and periodic structure theory, Technical Memorandum No. 959, Institute of Sound and Vibration Research, University of Southampton, March 2006.
[29] D. Weinberg, Development and comparison of the CQUADR element in NEiNASTRAN, online.
[30] D.J. Mead, *Passive Vibration Control*, Wiley, Chichester, 1998.
[31] B.R. Mace, Periodically stiffened fluid-loaded plates, II: response to line and point forces, *Journal of Sound and Vibration* 73 (4) (1980) 487–504.
[32] Y.Y. Pang, Modelling Acoustic Properties of Trusslike Periodic Panels: Application to Extruded Aluminium Profiles for Rail Vehicles, Master's Thesis, KTH Stockholm, Sweden, 2004.
[33] C. Hoever, Experimental evaluation of dispersion characteristics, Project Report, Institute of Fluid Mechanics and Engineering Acoustics, Technische Universität Berlin, Germany, December 2007.